ARTICLE

doi:10.1038/nature10922

A new hominin foot from Ethiopia shows multiple Pliocene bipedal adaptations

Yohannes Haile-Selassie[1,2], Beverly Z. Saylor[2], Alan Deino[3], Naomi E. Levin[4], Mulugeta Alene[5] & Bruce M. Latimer[2]

A newly discovered partial hominin foot skeleton from eastern Africa indicates the presence of more than one hominin locomotor adaptation at the beginning of the Late Pliocene epoch. Here we show that new pedal elements, dated to about 3.4 million years ago, belong to a species that does not match the contemporaneous *Australopithecus afarensis* in its morphology and inferred locomotor adaptations, but instead are more similar to the earlier *Ardipithecus ramidus* in possessing an opposable great toe. This not only indicates the presence of more than one hominin species at the beginning of the Late Pliocene of eastern Africa, but also indicates the persistence of a species with *Ar. ramidus*-like locomotor adaptation into the Late Pliocene.

Woranso-Mille is a relatively new palaeontological site located in the central Afar region of Ethiopia[1]. The fossiliferous horizons identified at the site range in age from approximately 3.2 to 3.8 million years (Myr) ago. More than 54,000 fossil specimens sampling diverse mammalian taxa have been collected thus far (Supplementary Information). Geological and palaeontological work in the past five years has concentrated on sediments radiometrically dated to between 3.57 ± 0.014 and 3.8 ± 0.18 Myr ago[2]. These sediments have yielded numerous early hominin remains, including a partial skeleton of *Au. afarensis*[3–5]. Slightly younger deposits have subsequently yielded hominin fossils including a well-preserved, ~3.4-Myr-old partial foot skeleton (BRT-VP-2/73). The detailed geological context, dating and palaeoenvironment of BRT-VP-2/73 are presented in the Supplementary Information.

The hominin forefoot (metatarsals and phalanges) is characteristically under-represented in the fossil record as a consequence of its fragility in the face of predators and taphonomic processes. Previously described hominin pedal fossils[6–12] have not included associated and well-preserved metatarsals and phalanges. Here we describe a partial hominin forefoot (BRT-VP-2/73) recovered from Burtele locality 2 (BRT-VP-2), one of the vertebrate localities of the Woranso-Mille study area (see Fig. 1). This partial pedal skeleton is unique in providing important evidence bearing on the functional morphology and proportions of several early hominin foot elements. It also presents the opportunity to draw morphological and functional comparisons between earlier (*Ar. ramidus*, ~4.4 Myr ago) and contemporaneous (*Au. afarensis*, ~2.9–3.6 Myr ago) hominins, and test whether there was diversity in hominin bipedalism in the earlier phases of hominin evolutionary history[13].

BRT-VP-2/73 consists of eight mostly intact bony elements of a right foot: complete first, second, fourth metatarsals; head of third metatarsal; three proximal phalanges (rays 1, 2 and 4); and one middle phalanx (ray 2) (Fig. 2a–f and Table 1). Detailed comparative descriptions are provided in Supplementary Information. The lack of anatomical redundancy, spatial distribution, individual age status, morphological compatibility and preservation of the specimens indicate that they are from a single foot.

BRT-VP-2/73 clearly differs from cercopithecids by its dorsoplantarly tall hallucal base relative to the bone's length (Fig. 3a) and also relative to the height of the second metatarsal base (Fig. 3b), in addition to a number of other metatarsal ratios (Fig. 4, see Supplementary Information for discussions). Principal components analysis (PCA; correlation matrix, varimax rotation with Kaiser normalization) was conducted on 11 metatarsal ratios (Supplementary Table 1). Although some metatarsal length proportions of BRT-VP-2/73 are more similar to those of cercopithecids (for example, MT2 length < MT4 length) than those

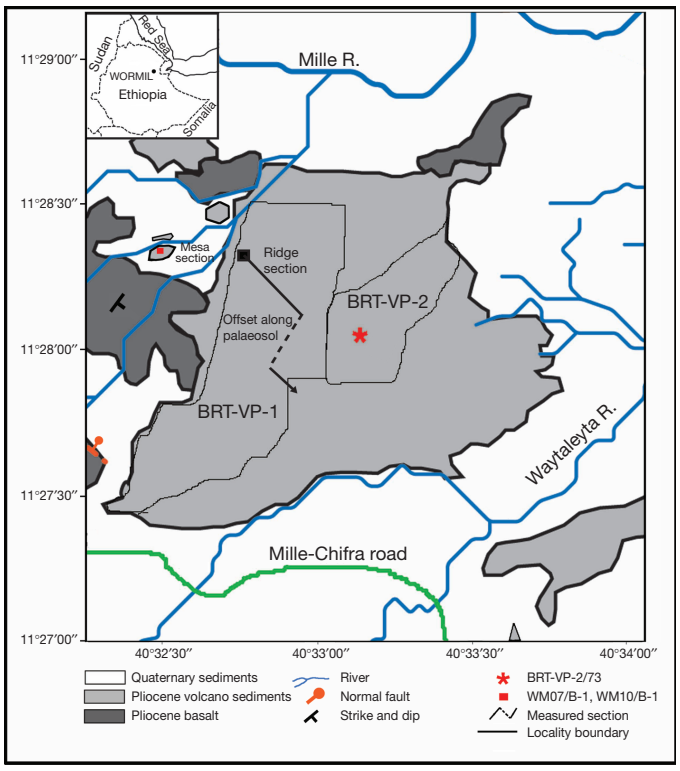

Figure 1 | Location map of the Burtele (BRT) vertebrate localities (BRT-VP-1 and BRT-VP-2) in the Woranso-Mille study area. The path of the measured section through the sandstone ridges and the location of the mesa section with the dated Burtele tuff are shown. The measured basalt section is off the map. The study area is located about 30 miles north of Hadar and Gona.

[1]The Cleveland Museum of Natural History, Cleveland, Ohio 44106, USA. [2]Case Western Reserve University, Cleveland, Ohio 44106, USA. [3]Berkeley Geochronology Center, Berkeley, California 94720, USA. [4]Johns Hopkins University, Baltimore, Maryland 21218, USA. [5]Addis Ababa University, PO Box 1176 Addis Ababa, Ethiopia.

Figure 2 | Pedal elements of BRT-VP-2/73. **a**, Dorsal view of all elements of the specimen. **b**, Dorsal, plantar, lateral, medial, distal and proximal views of the first metatarsal. **c**, Dorsal, lateral, medial, proximal and distal views of the second metatarsal. **d**, Dorsal, lateral, plantar, distal and proximal views of the hallucal proximal phalanx. **e**, Lateral views of the second and fourth proximal phalanges, and the second intermediate phalanx. **f**, Dorsal, plantar and lateral views of the fourth metatarsal. All views are from left to right.

of apes or humans, the results of the PCA clearly distinguish BRT-VP-2/73 from Old World monkeys and show that it falls in the cluster formed by anatomically modern humans and gorillas (Fig. 4 and Supplementary Information).

The proximal phalanges of BRT-VP-2/73 show the pronounced dorsal canting associated with substantial doming of its metatarsal heads similar to the condition seen in humans and early hominins such as *Ar. ramidus* and *Au. afarensis*. BRT-VP-2/73 differs from chimpanzees by lacking long and curved metatarsal shafts (Supplementary Fig. 1) and phalanges, and in having a larger degree of dorsiflexion at the lateral metatarsophalangeal joints. It also differs from African apes by the degree of torsion of its hallucal head (Supplementary Fig. 2) and doming of its second and fourth metatarsal heads. BRT-VP-2/73 is similar to *Ar. ramidus* in showing a mosaic of derived hominin pedal characteristics associated with obligate bipedality and other features associated with arboreality. For example, it resembles *Ar. ramidus* in combining an abducent hallux and medially directed torsion of the second metatarsal. However, its attribution to this species would be premature particularly in the absence of associated craniodental elements.

Comparative description

The hallux is represented by a complete, well-preserved, right first metatarsal (BRT-VP-2/73c) and its associated proximal phalanx (BRT-VP-2/73g; Fig. 2a, b, d). The articular base of the metatarsal is tall, deeply concave, and it exhibits the sigmoidal configuration seen in extant African apes and in *Ar. ramidus*[11]. There is a low ridge running obliquely across the proximal articular surface from its medial dorsoplantar midpoint to the attachment area of the fibularis longus. A similar feature sometimes occurs in *Gorilla* hallucal metatarsals. This subdued ridge is not like that described in the proximal metatarsal base from Hadar, Ethiopia (A.L. 333-54) wherein a distinct elevation nearly horizontally bisects the articular base into two semicircular facets[14]. The BRT-VP-2/73c base is notably tall relative to the bone's length, exceeding the ranges in chimpanzees and Old World monkeys, but within the ranges of gorillas and anatomically modern humans for this ratio (Fig. 3a).

The BRT-VP-2/73c metatarsal head does not conform to the 'typical' *Australopithecus* pattern in lacking the dramatic dorsal doming that characterizes this genus[6,14] (for example, A.L. 333-115a and A.L. 333-21).

Table 1 | Linear measurements of the pedal elements of BRT-VP-2/73

Specimen no.	Element	M1 (mm)	M2 (mm)	M3 (mm)	M4 (mm)	M5 (mm)	M6 (mm)	M7 (mm)	M8 (°)
BRT-VP-2/73a	R. MT4	68.7	12.7	13.3	10.5	12.1	5.4	9.2	26–27†
BRT-VP-2/73b	R. MT2	66.9	12.8	14.2	9.8	11.2	6.05	7.35	23‡
BRT-VP-2/73c	R. MT1	50.3	14.6	22.7	16.7	14.5	9.05	8.95	–
BRT-VP-2/73d	R. prox. PHX 4	28.74	10.25	8.6	7.9	5.4	5.32	5.16	–
BRT-VP-2/73e	R. prox. PHX 2	29.7	10.9	9.6	7.95	5.3	6.35	6.02	–
BRT-VP-2/73f	R. MT3 head	15.1*	–	–	8.6*	13.2*	–	–	–
BRT-VP-2/73g	R. prox. PHX 1	25.23	13.1	9.73	12.24	6.5	8.45	6.06	–
BRT-VP-2/73h	R. Int. PHX 2	18.5	9.26	7.63	7.3	4.4	5.1	3.85	–

M1, maximum length; M2, proximal articular joint mediolateral; M3, proximal articular joint dorsoplantar; M4, distal articular joint mediolateral; M5, distal articular joint dorsoplantar; M6, midshaft mediolateral; M7, midshaft dorsoplantar; M8, distal head torsion.
* Preserved dimension.
† Lateral torsion in degrees.
‡ Medial torsion in degrees.

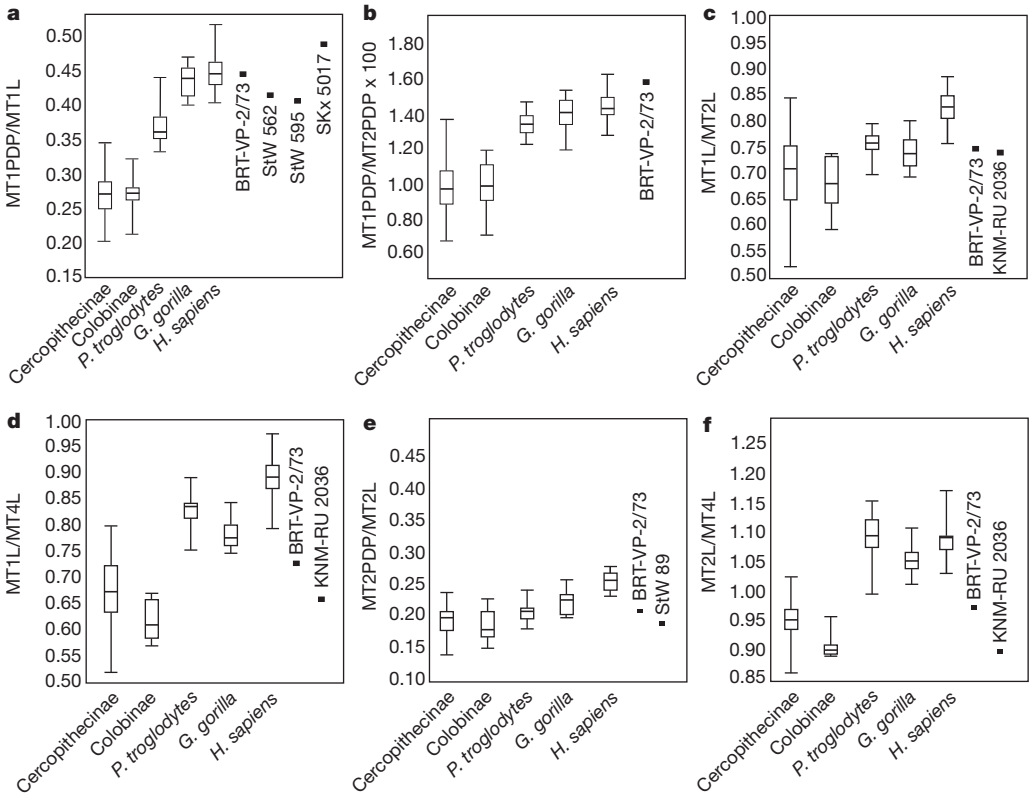

Figure 3 | Box-and-whisker plots of pedal element comparative ratios in cercopithecines, colobines, chimpanzees, gorillas, humans and fossil specimens. (See Supplementary Table 6 for taxonomic composition.) Whisker lines indicate maximum and minimum values. **a**, Base height (PDP) of the first metatarsal to its length (L). **b**, Base height of the first metatarsal to base height of the second metatarsal. **c**, Hallucal length to the second metatarsal length. **d**, Hallucal length to the fourth metatarsal length. **e**, Base height of the second metatarsal to its length. **f**, Length of the second metatarsal to the length of the fourth metatarsal. Measurements of the South African and Miocene hominoids were taken from refs 10 and 17, respectively.

Its dorsoproximal articular margin is continuous and it does not exhibit the 'nonsubchondral isthmus' described in *Ar. ramidus*[11].

A simple ratio comparing the length of the first metatarsal to the lengths of the second and fourth metatarsals demonstrates that the hallucal segment is relatively short, falling within the ranges of the African apes (Fig. 3c, d) and outside the range for anatomically modern humans (Supplementary Table 2). However, its tall hallucal base, relative to the shorter bases of the associated metatarsals, indicates that the BRT foot had a transverse arch more developed than in apes and falls in this ratio at the higher range for anatomically modern humans (Fig. 3a).

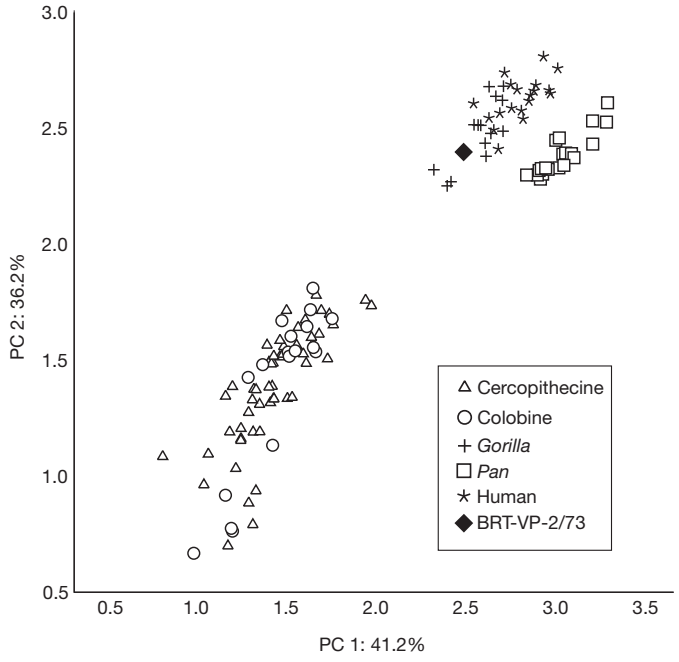

Figure 4 | Principal component analysis (PCA) of metatarsal ratios. Both PC1 and PC2 for 11 metatarsal ratios (descriptions of the ratios are provided in Supplementary Table 1) discriminate anatomically modern humans and apes from monkeys on the one hand and chimpanzees from anatomically modern humans and gorillas on the other. BRT-VP-2/73 falls in the human/gorilla cluster. Both components are heavily influenced by ratios 6, 9 and 10, which are all associated exclusively with dimensions of the hallux (see Supplementary Information for further discussion).

The hallucal proximal phalanx is essentially complete and, when combined with its associated metatarsal, further confirms that the hallucal ray is relatively short. A ratio formed between the combined lengths of the first metatarsal and its associated proximal phalanx (MT1 + PP1) and the same elements from the second ray (MT2 + PP2) demonstrates that anatomically modern humans with their elongated halluces are notably distinct. BRT-VP-2/73c falls within the ranges of apes and monkeys, indicating that the foot had a relatively short, abductable great toe (Supplementary Fig. 3). This ratio also confirms that the BRT-VP-2/73 hallucal ray was not used during a human-like toe-off in the terminal phase of the gait cycle. However, the degree of its proximal joint canting (97°) is lower than in the second ray (100°), which is a condition seen in humans, whereas the opposite is the case in chimpanzees[15] (Supplementary Fig. 4a).

The second ray is represented by a metatarsal (BRT-VP-2/73b), a proximal phalanx (BRT-VP-2/73e) and an intermediate phalanx (BRT-VP-2/73h). BRT-VP-2/73b is a well-preserved second metatarsal. The proximal base is triangular in outline. In lateral view, the base is slightly rounded in profile (distally directed concavity) and the shaft is longitudinally curved (Fig. 2c). Relative to the bone's overall length the dorsoplantar basal height is compressed, falling below the average for *Pan*, *Gorilla*, anatomically modern humans (Fig. 3e), and the single reported *Ar. ramidus* sample (see supplementary figure 4 in ref. 11). The dorsum of the BRT-VP-2/73 base does not exhibit the two 'chondral invaginations' described for *Ar. ramidus*[11].

Torsion along the shaft results in the long axis of the articular head being oriented about 23° medially from the dorsoplantar axis of the base. This torsion towards the hallux is on average less than that seen in *Pan* and *Gorilla*, but significantly more than that seen in anatomically

modern humans (on average this torsion ranges from neutral to 1–5 degrees (Supplementary Fig. 2)). In dorsal view (Fig. 2c), the shaft curves towards the medial side of the foot, a feature that in combination with the aforementioned axial torsion acts to further direct the articular head towards the hallux. This complex is characteristic of extant African apes and *Ar. ramidus* and is indicative of a grasping great toe.

In contrast to the hallucal metatarsal, the superior surface morphology of the articular head of the second metatarsal does conform to the 'typical' morphological pattern shared by *Ardipithecus* and *Australopithecus*[6,12,16]. In distal view, the head is roughly triangular in shape and its rounded dorsal apex is domed above the epiphyseal junction. This dorsal doming creates the distinctive transverse gutter between the subchondral margin and the diaphysis, indicating the passive hyperdorsiflexion at the metatarsophalangeal joint that occurs during bipedal heel-off through toe-off[11,16].

The articulating second proximal (BRT-VP-2/73e) and intermediate (BRT-VP-2/73h) phalanges also exhibit the derived anatomical features shared with *Ar. ramidus*[11] and *Au. afarensis*[6,12]. The base of the proximal phalanx exhibits the dorsiflexive anterior cant (100°) conforming to the dorsiflexion dome of the associated metatarsal head. Like *Ar. ramidus* and *Au. afarensis*, the shaft exhibits strong curvature, although not as much as in chimpanzees (Fig. 2e and Supplementary Fig. 4b; see also Supplementary Information for angle measurement methods and discussions). The inclination of the proximal articular surface in combination with the bone's longitudinal curvature results in the characteristic sulcus on the dorsal surface where the articular surface joins the shaft. The second intermediate phalanx (BRT-VP-2/73h) is relatively long compared to the associated proximal phalanx (Supplementary Table 3).

The third ray (BRT-VP-2/73f) is represented only by an isolated metatarsal head (see Fig. 2a). It too conforms to the pattern seen in *Ardipithecus*[11] and *Australopithecus*[6] (Supplementary Fig. 5) in exhibiting dorsal doming. The dorsoplantar height of the third metatarsal head exceeds that of the second metatarsal, a relationship more common in *Pan*, *Gorilla* and *Australopithecus* than in anatomically modern humans wherein the second metatarsal head is usually taller (Supplementary Table 2).

The fourth ray is represented by a complete metatarsal (BRT-VP 2/73g) and its associated proximal phalanx (BRT-VP 2/73d; Fig. 2e, f). A ratio of the estimated dorsoplantar height of the metatarsal base and the bone's length indicates that the fourth metatarsal does not have the expanded, stabilizing base morphology seen in *Au. afarensis*[12] and *Homo* but, rather, is similar to *Pan* and some Old World monkeys (Supplementary Fig. 6).

The most unexpected feature seen in the fourth metatarsal is its relative length when compared to the associated first and second metatarsals. The fourth metatarsal is absolutely longer than is the second metatarsal, a condition not previously encountered in extant apes or hominins. The fourth metatarsal is also much longer than is the hallucal metatarsal and in this ratio, the fossil specimen again fails to align with extant apes or hominins and is most similar to Old World monkeys (Fig. 3d, f). At present, no associated fossil elements allow a similar comparison in *Ardipithecus* or *Australopithecus* and, as a consequence, no judgment can be reliably made regarding the polarity of this character. A relatively longer fourth metatarsal is the usual condition in Old World monkeys and it also occurs in some Miocene apes (KNM-RU 2036; ref. 17), indicating that it probably represents the primitive condition.

The proximal phalanx of the fourth ray (BRT-VP-2/73d; Fig. 2e) is well preserved and similar to those observed in *Ardipithecus*[11] and *Australopithecus*[6,16]. It has the shallow transverse sulcus where the proximal articular surface cants anteriorly into the curvature of the shaft. It presents a higher degree of dorsal canting than does the phalanx of the second ray (104°, see Supplementary Fig. 4a and Supplementary Information for discussions).

Implications for hominin pedal evolution

Comparisons with the earlier *Ar. ramidus* and contemporaneous *Au. afarensis* provide a morphological and chronological context within which to view BRT-VP-2/73. Several relevant pedal elements are also represented in the South African samples from Sterkfontein and Swartkrans[10] (see Supplementary Information for further discussion).

The earlier *Ar. ramidus* pedal remains indicate a mosaic foot capable of terrestrial bipedal toeing-off on the lateral four metatarsophalangeal joints (oblique metatarsal axis[11]) while still maintaining a functionally abductable, grasping hallux. By contrast, the foot of *Au. afarensis* possessed a longitudinal pedal arch[6,12,18], a permanently adducted great toe[12,14,16], dorsal doming of its hallucal head[6,14], anteriorly canted bases on its proximal phalanges[6,16] (also shared by *Ar. ramidus*[11]), and clearly used a human-like transverse metatarsal axis during the latter stages of toe-off.

Although BRT-VP-2/73 is contemporaneous with *Au. afarensis* at around 3.4 Myr ago (see Fig. 5), it differs significantly from the known feet of *Australopithecus*. Its hallux is short and the hallucal metatarsal head lacks dorsal doming. The bases of the second and fourth metatarsals of BRT-VP-2/73 do not have the expanded dorsoplantar dimensions seen in *Ardipithecus*[11] and *Australopithecus*[12,14], features that along with the associated rugose ligamentous attachments would resist midtarsal and tarsometatarsal dorsiflexion and midfoot breaking[19–23]. However, its lateral metatarsophalangeal joints (MTs 2, 3 and 4) do conform morphologically to the *Ardipithecus* and *Australopithecus* pattern, in having dorsally domed heads and an anterior cant to the phalangeal bases.

BRT-VP-2/73 also resembles *Ar. ramidus* in combining an abducent hallux and the medially directed torsion of the second metatarsal. It is also similar to *Ar. ramidus* and *Au. afarensis* in the metatarsophalangeal joints of the other rays, indicating that these adaptations in the lateral foot are among the earliest anatomical modifications to hominin terrestrial bipedality. The height of the hallucal metatarsal base suggests that a well-developed transverse pedal arch preceded the development of a permanent longitudinal arch. However, the lack of dorsoplantar expansion of the metatarsal bases (MTs 2 and 4) suggests that this midtarsal stabilizing feature seen in both *Ar. ramidus*[11] and *Au. afarensis*[12] was absent in this specimen.

The most surprising feature observed in the BRT-VP-2/73 forefoot is the length of the fourth metatarsal relative to the first and second metatarsals. The currently available *Ardipithecus* and *Australopithecus* (eastern and South African) fossil record is not adequate to assess accurately the significance of this particular feature. However, in light of its occurrence in some Miocene apes (for example, KNM-RU 2036) it may represent the primitive state in early hominins. Nonetheless, it is clear that the BRT-VP-2/73 foot skeleton represents a hominin that, unlike the contemporaneous *Au. afarensis*, retained a grasping capacity that would allow it to exploit arboreal settings more effectively. Yet, judging from its lateral metatarsophalangeal complex, when on the ground it was at least facultatively bipedal, although it may have practiced bipedality in a novel fashion probably similar to *Ar. ramidus*. Unlike *Au. afarensis*, it did not have a longitudinal pedal arch, nor was it capable of efficiently using the transverse metatarsal axis.

Although the taxonomic affinity of BRT-VP-2/73 is currently indeterminate, there is adequate morphological evidence that it does not belong to the contemporaneous species *Au. afarensis*. Regardless of its taxonomic affinity, however, this specimen is the first strong evidence indicating multiple hominin lineages, adaptively separated (at least in the foot skeleton), in the 3–4-Myr-ago time interval. A final, but important, note for the metatarsal ratios used in the PCA performed in this study, anatomically modern humans and gorillas overlap substantially and BRT-VP-2/73 falls in the gorilla cluster. It is unclear at this point what the functional implications of this overlap might mean; it requires further investigation as it has important consequences for the interpretation of locomotor behaviour in early hominins.

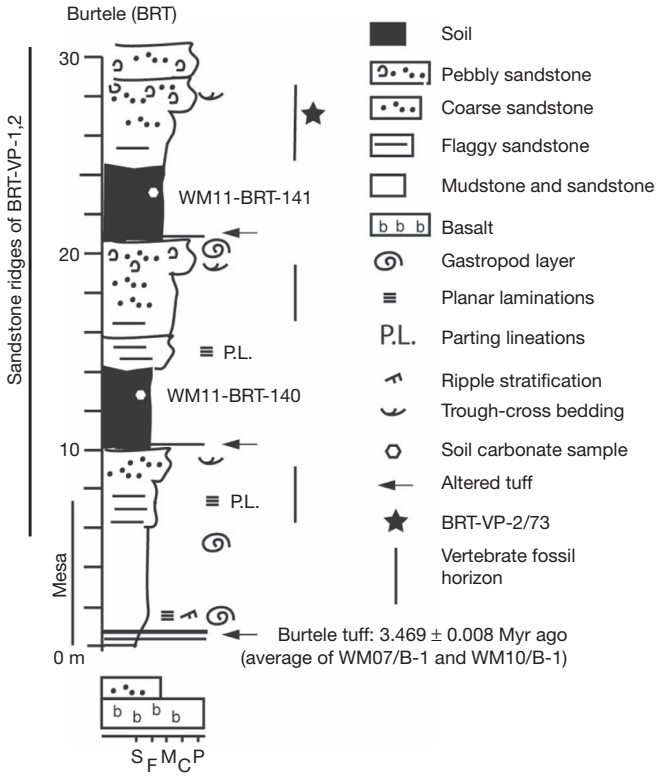

Figure 5 | Stratigraphic section at the BRT localities and placement of the BRT-VP-2/73 partial foot skeleton. The Burtele tuff is dated by the $^{40}Ar/^{39}Ar$ method to 3.469 ± 0.008 Myr ago and lies a maximum of about 27 m below BRT-VP-2/73, providing a maximum age constraint of ~3.47 Myr ago for the foot specimen (shown by the black star) and for three fossiliferous sandstone horizons (shown by vertical lines) at BRT-VP-1 and BRT-VP-2. An approximate age for the foot specimen, using regional sediment accumulation rates, suggests an age of between 3.2 and 3.4 Myr ago for BRT-VP-2/73 (see Methods for details). S, F, M, C, P indicates soil, flaggy, mudstone, coarse and pebbly sandstone, respectively; it shows the degree of resistance to erosion and rock stiffness.

METHODS SUMMARY

The Burtele tuff at the base of the section is dated by the $^{40}Ar/^{39}Ar$ method to 3.469 ± 0.008 Myr ago (analytical data are given in Supplementary Information) and lies a maximum of about 27 m below BRT-VP-2/73, providing a firm maximum age constraint of ~3.47 Myr ago for the foot specimen (Fig. 5). An approximate age for the foot specimen can be estimated using regional sediment accumulation rates. The average rate for older WORMIL strata in the Waki-Mille confluence area is 11 cm kyr^{-1} (ref. 2), which yields an estimated age of 3.22 Myr ago for the BRT-VP-2/73 specimen. This rate is much lower than estimates for the Sidi Hakoma Member of the Hadar Formation[24–26], which is closer in age to the BRT ridge section, but is much farther away geographically. Using a Sidi Hakoma accumulation rate of 30 cm kyr^{-1} yields an estimate of 3.38 Myr ago for BRT-VP-2/73. These contrasting rates indicate an age of between 3.2 and 3.4 Myr ago for BRT-VP-2/73.

For the isotopic analysis of pedogenic carbonate, carbonate nodules were sampled from peds with slickenside surfaces and clay cutans, within a distinct pedogenic carbonate zone, ≥50 cm below the palaeosol contact with the overlying silt. $\delta^{13}C$, $\delta^{18}O$ and Δ_{47} measurements of carbonate were made using an automated common acid bath peripheral coupled to a Thermo MAT 253 mass spectrometer at Johns Hopkins University, using methods described previously[27]. The results are reported in Supplementary Table 8.

Full Methods and any associated references are available in the online version of the paper at www.nature.com/nature.

Received 22 October 2011; accepted 8 February 2012.

1. Haile-Selassie, Y., Deino, A., Saylor, B., Umer, M. & Latimer, B. Preliminary geology and paleontology of new hominid-bearing Pliocene localities in the central Afar region of Ethiopia. *Anthropol. Sci.* **115,** 215–222 (2007).
2. Deino, A. L. *et al.* $^{40}Ar/^{39}Ar$ dating, paleomagnetism, and tephrochemistry of Pliocene strata of the hominid-bearing Woranso-Mille area, west-central Afar Rift, Ethiopia. *J. Hum. Evol.* **58,** 111–126 (2010).
3. Haile-Selassie, Y., Saylor, B. Z., Deino, A., Alene, M. & Latimer, B. New hominid fossils from Woranso-Mille (Central Afar, Ethiopia) the taxonomy of early *Australopithecus*. *Am. J. Phys. Anthropol.* **141,** 406–417 (2009).
4. Haile-Selassie, Y. *et al.* An early *Australopithecus afarensis* postcranium from Woranso-Mille, Ethiopia. *Proc. Natl Acad. Sci. USA* **107,** 12121–12126 (2010).
5. Haile-Selassie, Y. Phylogeny of early *Australopithecus*: new fossil evidence from the Woranso-Mille (Central Afar, Ethiopia). *Phil. Trans. R. Soc. B* **365,** 3323–3331 (2010).
6. Latimer, B. M. & Lovejoy, C. O. Hominid tarsal, metatarsal, and phalangeal bones recovered from the Hadar formation: 1974–1977 collections. *Am. J. Phys. Anthropol.* **57,** 701–719 (1982).
7. Day, M. H. & Napier, J. R. Hominid fossils from Bed I, Olduvai Gorge, Tanganyika: fossil footbones. *Nature* **201,** 969–970 (1964).
8. Zipfel, B. *et al.* The foot and ankle of *Australopithecus sediba*. *Science* **333,** 1417–1420 (2011).
9. Clarke, R. J. & Tobias, P. V. Sterkfontein Member 2 foot bones of the oldest South African hominid. *Science* **269,** 521–524 (1995).
10. Deloison, Y. Anatomie des os fossiles de pieds des hominides d'Afrique du Sud. *Biomet. Hum. Anthropol.* **21,** 189–230 (2003).
11. Lovejoy, O. C., Latimer, B., Suwa, G., Asfaw, B. & White, T. D. Combining prehension and propulsion: The foot of *Ardipithecus ramidus*. *Science* **326,** 72 (2009).
12. Ward, C. V., Kimbel, W. H. & Johanson, D. C. Complete fourth metatarsal and arches in the foot of *Australopithecus afarensis*. *Science* **331,** 750–753 (2011).
13. Harcourt-Smith, W. E. H. & Aiello, L. C. Fossils, feet and the evolution of human bipedal locomotion. *J. Anat.* **204,** 403–416 (2004).
14. Latimer, B. M. & Lovejoy, C. O. Hallucal tarsometatarsal joint in *Australopithecus afarensis*. *Am. J. Phys. Anthropol.* **82,** 125–133 (1990).
15. Griffin, N. L. & Richmond, B. G. Joint orientation and function in great ape and human proximal pedal phalanges. *Am. J. Phys. Anthropol.* **141,** 116–123 (2010).
16. Latimer, B. M. & Lovejoy, C. O. Metatarsophalangeal joints of *Australopithecus afarensis*. *Am. J. Phys. Anthropol.* **83,** 13–23 (1990).
17. Walker, A. C. & Pickford, M. in *New Interpretaions of Ape and Human Ancestry* (eds Ciochon, R. L. & Corruccini, R. S.) 325–413 (Plenum, 1983).
18. White, T. D. & Suwa, G. Hominid footprints at Laetoli: facts and interpretations. *Am. J. Phys. Anthropol.* **72,** 485–514 (1987).
19. Elftman, H. & Manter, J. Chimpanzee and human feet in bipedal walking. *Am. J. Phys. Anthropol.* **20,** 69–79 (1935).
20. Elftman, H. & Manter, J. The evolution of the human foot with special reference to the joints. *J. Anat.* **70,** 56–67 (1935).
21. DeSilva, J. M. Functional morphology of the ankle and the likelihood of climbing in early hominins. *Proc. Natl Acad. Sci. USA* **106,** 6567–6572 (2009).
22. D'Aout, K., Aerts, P., De Clercq, D., De Meester, K. & Van Elsacker, L. Segment and joint angles of hind limb during bipedal and quadrupedal walking of the bonobo (*Pan paniscus*). *Am. J. Phys. Anthropol.* **119,** 37–51 (2002).
23. Vereecke, E., D'Aout, K., De Clercq, D., Van Elsacker, L. & Aerts, P. Dynamic plantar pressure distribution during terrestrial locomotion of bonobos (*Pan paniscus*). *Am. J. Phys. Anthropol.* **120,** 373–383 (2003).
24. Walter, R. C. & Aronson, J. L. Age and source of the Sidi Hakoma Tuff, Hadar Formation, Ethiopia. *J. Hum. Evol.* **25,** 229–240 (1993).
25. deMenocal, P. B. & Brown, F. H. in *Hominid Evolution and Climatic Change in Europe* (eds Agusti, J., Rook, L. & Andrews, P.) 23–54 (Cambridge Univ. Press, 1999).
26. McDougall, I. & Brown, F. H. Geochronology of the pre-KBS Tuff sequence, Omo Group, Turkana Basin. *J. Geol. Soc. Lond.* **165,** 549–562 (2008).
27. Passey, B. H., Levin, N. E., Cerling, T. E., Brown, F. H. & Eiler, J. M. High-temperature environments of human evolution in East Africa based on bond ordering in paleosol carbonates. *Proc. Natl Acad. Sci. USA* **107,** 11245–11249 (2010).

Supplementary Information is linked to the online version of the paper at www.nature.com/nature.

Acknowledgements We thank the Authority for Research and Conservation of Cultural Heritage and the Afar Regional State of Ethiopia for permission to conduct field and laboratory research, and the Afar people of the Woranso-Mille area for support in the field. We also thank M. Asnake, R. Bernor, S. Frost, D. Geraads, I. Giaourtsakis, M. Lewis, W. Sanders and L. Werdelin for faunal identifications. We thank B. Passey for aid with isotope analyses; E. Guthrie for unpublished primary data; L. Russell for photography; S. Melillo and H. Gebreyesus for fieldwork; O. Lovejoy, S. Simpson, G. Suwa and T. White for comments and discussions; D. Su for discussions and assistance in statistical analysis; and L. Jellema for assistance in photography. This research was supported by funding from the LSB Leakey Foundation, the National Geographic Society, the Cleveland Museum of Natural History, and NSF grants BCS-0234320, BCS-0321893, BCS-0542037 and BCS-1124705.

Author Contributions Y.H.-S. and B.M.L. conducted the description and comparative analysis. B.Z.S., N.E.L. and M.A. compiled the stratigraphic sequence. A.D. conducted the radiometric dating. N.E.L. conducted stable isotope analysis. Y.H.-S. and B.M.L. wrote the paper with input from all authors.

Author Information Reprints and permissions information is available at www.nature.com/reprints. The authors declare no competing financial interests. Readers are welcome to comment on the online version of this article at www.nature.com/nature. Correspondence and requests for materials should be addressed to Y.H.-S. (yhailese@cmnh.org).

METHODS

$^{40}Ar/^{39}Ar$ dating procedures follow those of ref. 2. The mineral separates were irradiated for 5 h in two separate batches in the in-core CLICIT facility of the Oregon State University TRIGA reactor. Sanidine from the Fish Canyon Tuff of Colorado was used as a monitor mineral, with an age of 28.201 Myr[28]. After irradiation, the feldspar grains were individually analysed under ultra-high vacuum on a MAP 215 Noble-gas mass spectrometer, using a focused CO_2 laser as the heating device. In all, 56 grains were analysed from the two samples (Supplementary Table 7). Most grains (34) proved to be K-feldspar, as judged by the Ca/K ratio determined from the measured argon isotopes, whereas the remainder were relatively low-Ca/K plagioclase. Most analyses yielded the anticipated high proportion of radiogenic ^{40}Ar relative to atmospheric ^{40}Ar contamination expected for unaltered feldspars from Pliocene volcanic rocks, but a few exhibited anomalously low radiogenic content, and were excluded from further analysis; an arbitrary cutoff of 60% $^{40}Ar^*$ was used, identifying four grains for exclusion. In addition, as is typical for East African tephra, a slight tail of the age distribution towards older ages was observed. A statistical filter was applied to the sample distributions, using a median outlier determinant (outliers were classified as falling 1.5 'normalized median absolute deviations' from the median). Use of this criterion identified three outliers in each of WM07/B-1 (K-feldspar) and WM10/B-1 (Plagioclase). The remaining populations yield simple, unimodal Gaussian-like distributions (Supplementary Fig. 7). Weighted-mean sample ages of the K-feldspar populations from samples WM07/B-1 and WM10/B-1 are 3.484 ± 0.011 Myr ($n = 24$; 1σ analytical error, incorporating error in J, the neutron fluence parameter of 0.2%) and 3.453 ± 0.011 Myr ($n = 4$), respectively (Supplementary Table 4). An overall weighted-mean of the two K-feldspar ages is 3.469 ± 0.008 Myr, taken as the reference age for the Burtele tuff. The plagioclase weighted-mean age of sample WM10/B-1 is predictably less precise than either K-feldspar age, due to the lower potassium content, but is nevertheless a reasonable result (3.42 ± 0.03 Myr) that is not statistically different from the K-feldspar age.

The Burtele tuff at the base of the section is dated by the $^{40}Ar/^{39}Ar$ method to 3.469 ± 0.008 Myr ago (analytical data are given in Supplementary Information) and lies a maximum of about 27 m below BRT-VP-2/73, providing a firm maximum age constraint of ~3.47 Myr ago for the foot specimen. An approximate age for the foot specimen can be estimated using regional sediment accumulation rates. The average rate for older WORMIL strata in the Waki-Mille confluence area is 11 cm kyr^{-1} (ref. 2), which yields an estimated age of 3.22 Myr ago for the BRT-VP-2/73 specimen. This rate is much lower than estimates for the Sidi Hakoma Member of the Hadar Formation[24–26], which is closer in age to the BRT ridge section, but is much farther away geographically. Using a Sidi Hakoma accumulation rate of 30 cm kyr^{-1} yields an estimate of 3.38 Myr for BRT-VP-2/73. These contrasting rates suggest an age of between 3.2 and 3.4 Myr ago for BRT-VP-2/73.

For the isotopic analysis of pedogenic carbonate, carbonate nodules were sampled from peds with slickenside surfaces and clay cutans, within a distinct pedogenic carbonate zone, ≥50 cm below the palaeosol contact with the overlying silt. $\delta^{13}C$, $\delta^{18}O$ and Δ_{47} measurements of carbonate were made using an automated common acid bath peripheral coupled to a Thermo MAT 253 mass spectrometer at Johns Hopkins University, using methods described previously[27]. The results are reported in Supplementary Table 8.

28. Kuiper, K. F. *et al.* Synchronizing rock clocks of earth history. *Science* **320,** 500–504 (2008).

doi:10.1038/nature10922

Supplementary Figure 1. Dorsal (top row) and lateral (bottom row) views of metatarsals. **a,** Hallucal metatarsals. From left to right, *Theropithecus gelada, Pan troglodytes, Gorilla gorilla, Homo sapiens*, BRT-VP-2/73c, and Skx 5017. **b,** Second metatarsals. From left to right, *Theropithecus gelada, Pan troglodytes, Gorilla gorilla, Homo sapiens*, BRT-VP-2/73b, and Stw 89. Images of Skx 5017 and Stw 89 were taken from casts. All other images were taken from originals.

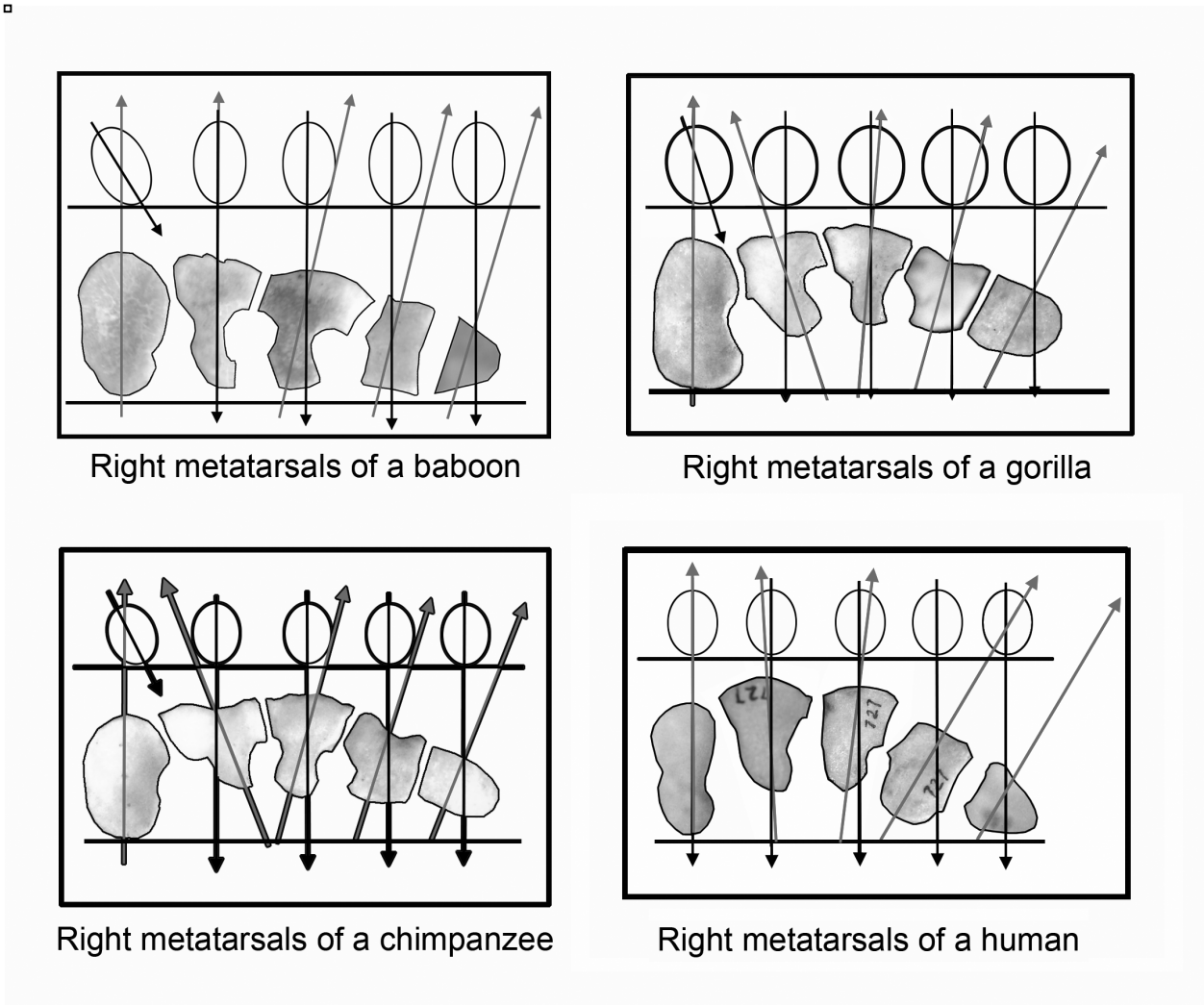

Supplementary Figure 2. Schematic metatarsal proximal (bottom) and distal (top) representations of baboons, gorillas, chimpanzees, and modern humans showing angular relations between the metatarsal head and its base. With the long axis of the metatarsal bases perpendicular to the substrate, the hallucal heads in baboons, gorillas and chimpanzees are comparatively torsioned medially, whereas in humans no torsion exists. Most importantly, however, humans have the deepest transverse arch compared to the apes with colobines possessing the shallowest transverse arch.

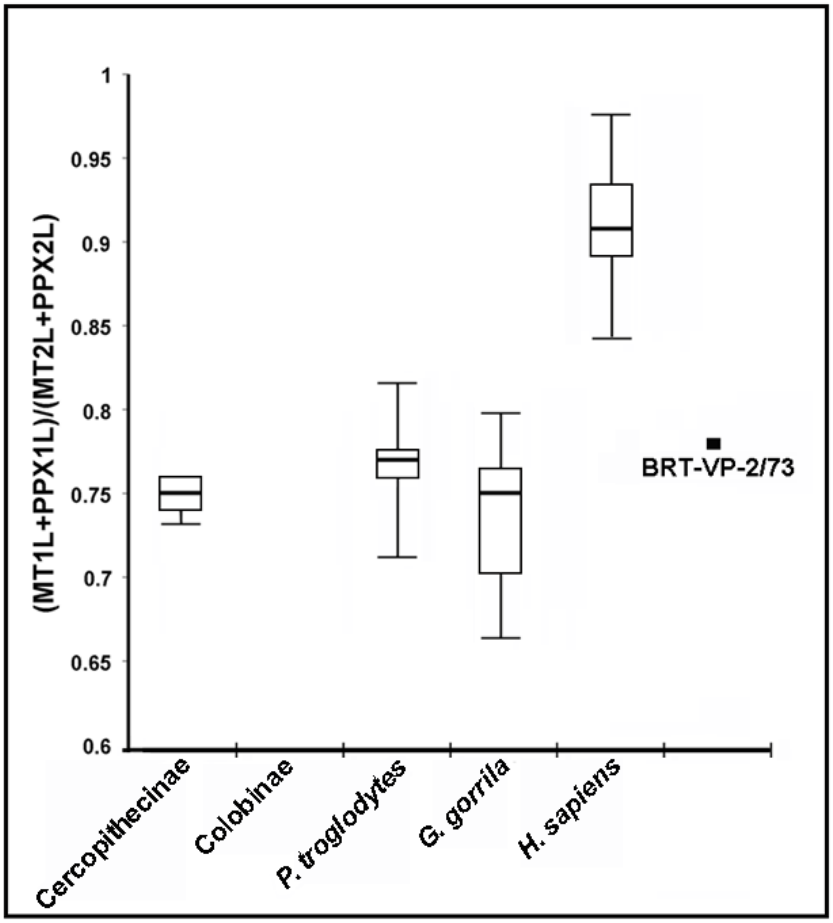

Supplementary Figure 3. Box-and-whisker plot of the ratio of the combined first metatarsal and its corresponding proximal phalanx lengths relative to the length of the combined second metatarsal and its corresponding proximal phalanx lengths. BRT-VP-2/73 falls on the higher range of chimpanzees and gorillas, but outside the range of modern humans, indicating that BRT-VP-2/73 had short first ray.

Supplementary Figure 4. **a**, degree of dorsal canting of the proximal phalanges (from left to right, ray 1, 2, and 4) of BRT-VP-2/73. The hallucal proximal phalanx is less dorsally canted than the corresponding second proximal phalanx as in humans and unlike chimpanzees (see ref. 15 for further discussions). The degrees were measured following the methods used in Ref. 15. **b**, second (top row) and fourth (bottom row) proximal phalangeal curvature in (from left to right) *Pan troglodytes*, BRT-VP-2/73, *Gorilla gorilla*, and *Homo sapiens*. Humans and gorillas have less curved phalanges than chimpanzees. The BRT-VP-2/73 phalanges are intermediate between the two groups.

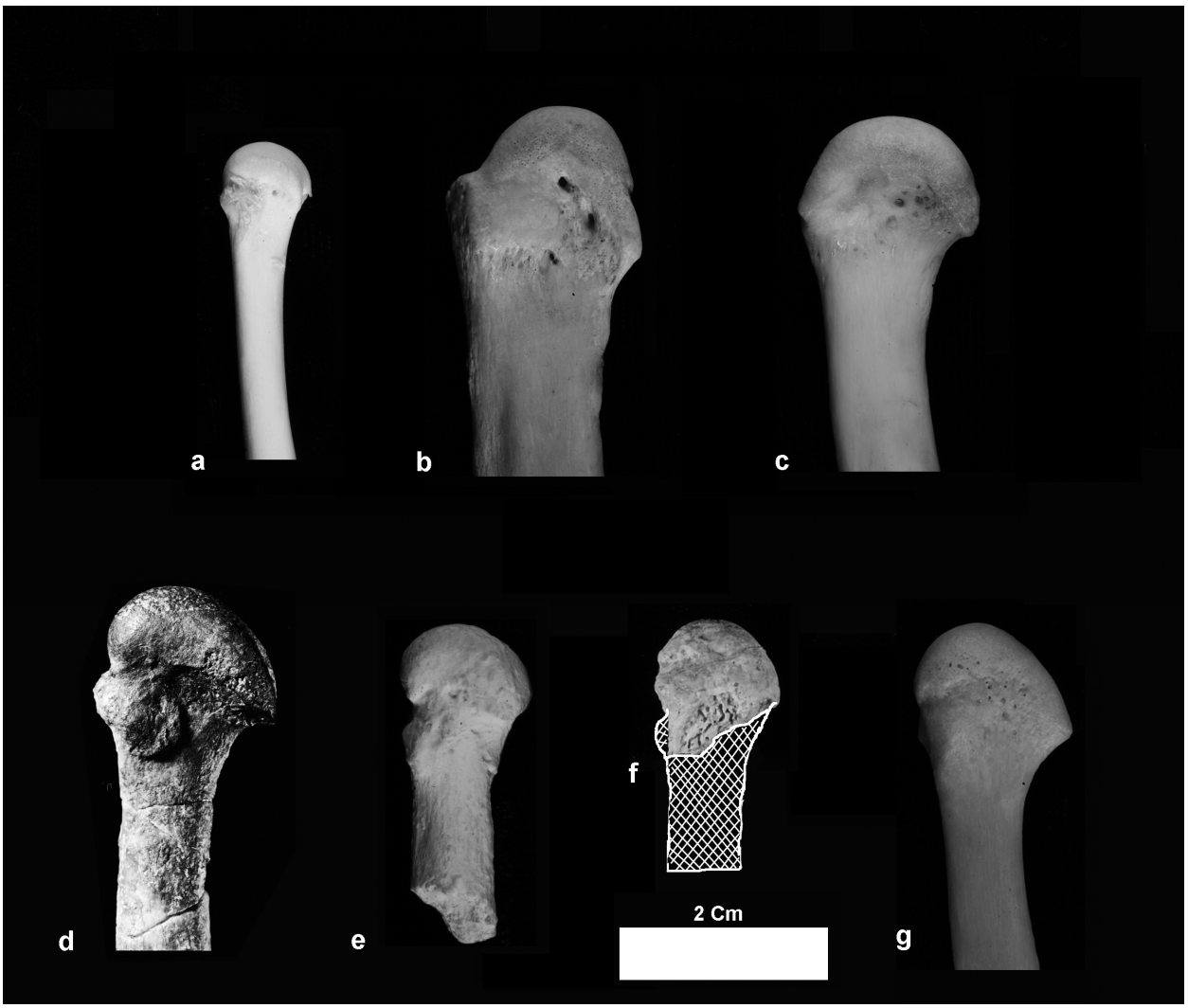

Supplementary Figure 5. Lateral view of the distal half of third metatarsals. **a**, *Theropithecus gelada*. **b**, *Gorilla gorilla*. **c**, *Pan troglodytes*. **d**, *Ardipithecus ramidus* (ARA-VP-6/505, reversed). **e**, *Australopithecus afarensis* (A.L. 333-72). **f**, BRT-VP-2/73f. **g**, *Homo sapiens*. Note that doming of the head is visible in all of the hominid specimens (bottom row), and absent in the apes and the cercopithecine. Images of (e) and (f) were taken from casts. The image of ARA-VP-6/505 is from Tim White. All other specimens are from the Cleveland Museum of Natural History's primate skeletal collection.

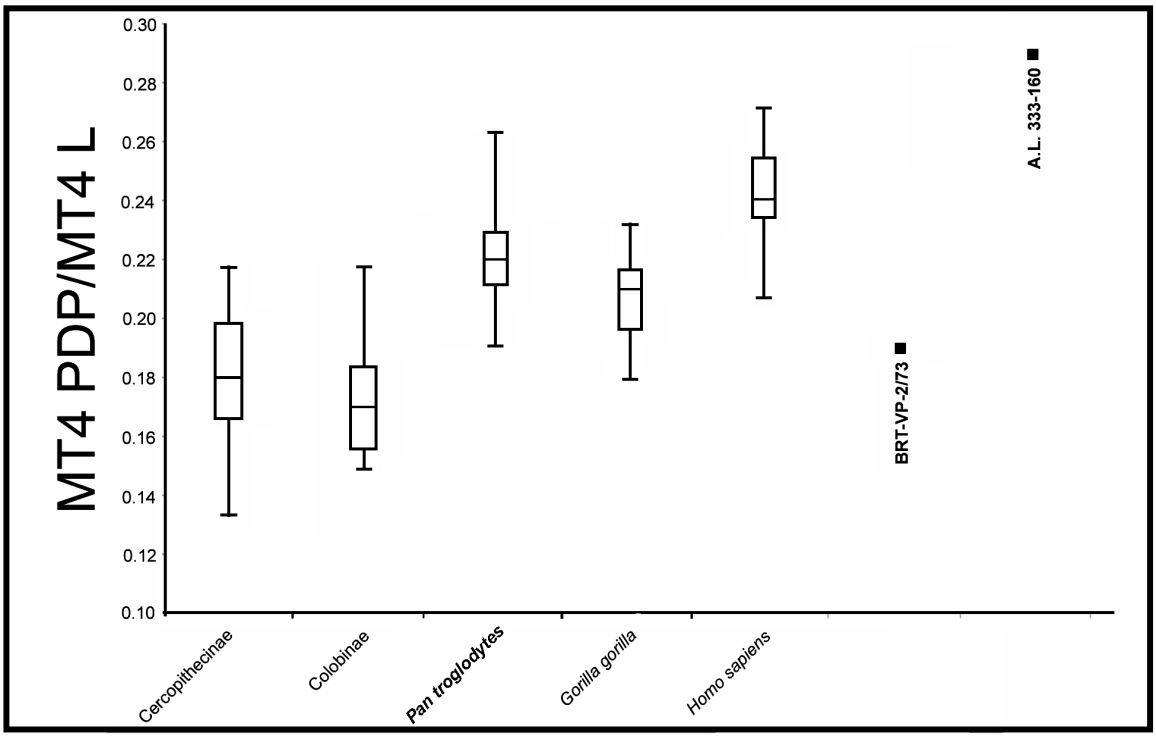

Supplementary Figure 6. Box-and-whisker plot of the ratio of the fourth metatarsal proximal base height (MT4PDP) relative to the length of the fourth metatarsal (MT4L). BRT-VP-2/73 falls outside the ranges of modern humans and chimpanzees and on the lower range of gorillas. It is more like the cercopithecines in this ratio. Measurements of A.L. 333-160 were taken from ref. 12.

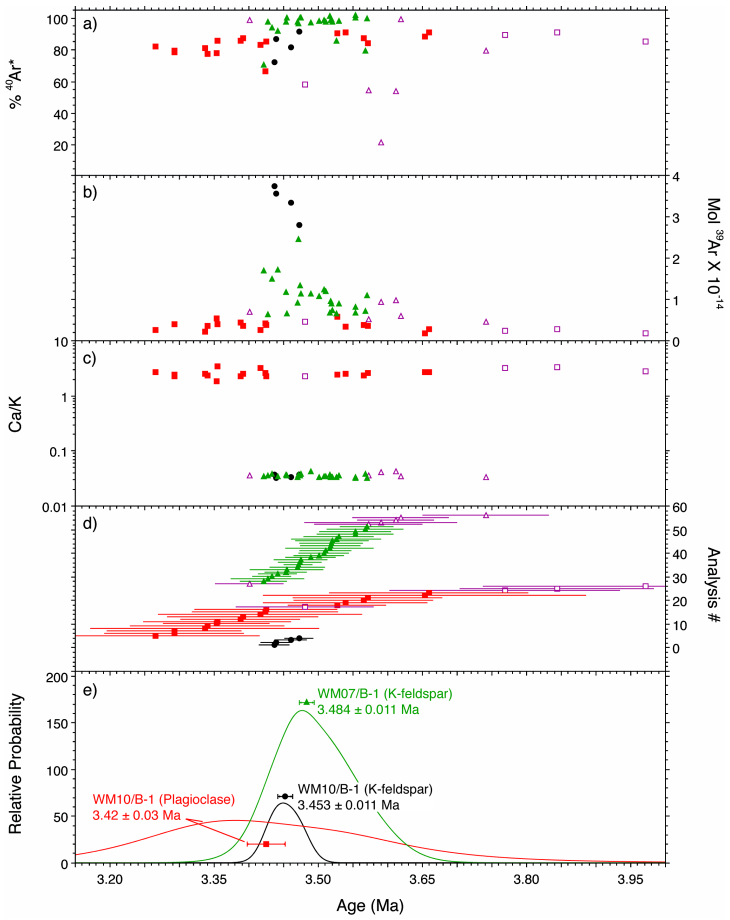

Supplementary Figure 7. Plots of analytical results and age-probability density spectra of plagioclase and K-feldspar single-grain $^{40}Ar/^{39}Ar$ dating of the Burtele tuff. Triangles: WM07/B-1 K-feldspar; Circles: WM10/B-1 K-feldspar; Squares: WM10/B-1 plagioclase. Open symbols represent excluded analyses. All plots are against age on the horizontal axis. a) $\%^{40}Ar^{*}$: percentage of radiogenic ^{40}Ar content as a total of radiogenic and atmospheric ^{40}Ar. b) moles of ^{39}Ar, c) Ca/K, d) individual analyses with 1s analytical uncertainty are shown by circles with horizontal error bars, ordered vertically by increasing age, e) age-probability density spectra. The weighted mean age and 1s analytical uncertainty (including error in *J*, the neutron fluence parameter) are shown numerically and by the appropriate symbol with error bars.

1. Discovery, geological context, and dating of BRT-VP-2/73

The first piece (proximal half of a fourth metatarsal) was discovered by Stephanie Melillo on February 15, 2009, eroding out of an unconsolidated sandstone horizon. Further surface scraping and excavation resulted in the recovery of the rest of the foot elements - a complete first metatarsal, a complete second metatarsal, the head of a third metatarsal, a complete fourth metatarsal, three proximal phalanges (rays 1, 2, and 4), and one intermediate phalanx (ray 2).

Localities BRT-VP-1 and BRT-VP-2 encompass low relief, NNE-SSW trending ridges composed primarily of eroding fine to pebbly sandstone. Basalt to the west of the localities forms a very gentle dip slope that extends the length of the topographic ridges and projects southeastward beneath them. Gaps in basalt exposure may be related to NW-SE striking faults, but any significant offset of the stratigraphic section has been ruled out by walking paleosol horizons along the length of, and between, ridges. Traced beds also tie the documented ridge section, which was measured through the best-exposed, thickest sandstone bodies in BRT-VP-1, to the specimen site in BRT-VP-2 (Figure 1).

BRT-VP-2/73 (the foot) was found below sandstone, approximately 27 meters stratigraphically above a thin, altered tuff, informally named the Burtele tuff. This tuff is exposed at the bottom of a mesa composed of upward-coarsening siltstone and fine sandstone. The facies transition at the top of the mesa, from silty sandstone to flaggy sandstone, is identical to facies at the bottom of the ridge section. Similar strata also are exposed 1 km south of the mesa, on the sides of a drainage floored by basalt, and these strata clearly extend eastward to the ridge section. Thus, although intervening Quaternary cover prevents walking beds between the mesa and ridge exposures, their similarity of facies and the absence of through-going faults are evidence that

they form a single continuous succession. That succession overlies basalt and consists of upward-coarsening sandstone with intervening recessive weathering paleosol horizons; it has the Burtele tuff near its base (Figure 4) and the BRT-VP-2/73 placement near its top. The stratigraphic succession is interpreted to have been deposited in a progradational deltaic environment.

Two samples of the Burtele tuff were dated by the single-crystal, laser-fusion $^{40}Ar/^{39}Ar$ method at the Berkeley Geochronology Center (see Methods below). The Burtele tuff samples were collected from the same mesa in 2007 (sample WM07/B-1; UTM 668218 m E, 1268787 m N, zone 37P) and 2010 (WM10/B-1). The sampled unit is a laterally uniform, 1-4 centimeter (cm) thick, devitrified white crystal fallout tuff containing up to 5% lithic fragments (to 3 millimeters (mm)), about 5% phenocrysts (to ~1 mm), and 5-10% fine pumice (<0.5 cm). The phenocryst population is dominated by subequal proportions of K-feldspar and plagioclase. The final mineral separates of the two samples emphasized different populations; WM07/B-1 was dominated by moderate sized K-feldspar, while WM10/B-1 contained larger grains, dominated about 5:1 by plagioclase. Weighted-mean $^{40}Ar/^{39}Ar$ ages of the K-feldspars from WM07/B-1 and WM10/B-1 are 3.484 ± 0.011 Myr (n = 24; 1s) and 3.453 ± 0.011 Myr (n = 4), respectively (see Supplementary Table 4).

An overall weighted-mean of the two K-feldspar ages is 3.469 ± 0.008 Myr, taken as the reference age for the Burtele tuff. The plagioclase weighted-mean age of sample WM10/B-1 is predictably less precise than either K-feldspar age, due to the lower potassium content, but is nevertheless a reasonable result (3.42 ± 0.03 Myr) that is not statistically different from the K-feldspar age (Supplementary Figure 7; Supplementary Table 4).

The Burtele tuff is slightly older than the widespread Sidi-Hakoma Tuff recognized within the Hadar Formation ('SHT'; 3.44 ± 0.03 Myr[24], age updated for consistency with the monitor age used herein), which is equivalent to the Tulu Bor Tuff of the Turkana Basin (3.41 ± 0.01 Myr orbitally tuned age[25] and maximum depositional age of 3.45 ± 0.023 Myr[26], updated for monitor age). In addition to the age difference, the coarse mineralogy, abundance of lithic fragments, and the presence of pumice in the Burtele tuff indicate that this unit is derived from nearby volcanism and is likely not of extrabasinal origin.

2. Supplementary Description

2.1. The first ray

The proximal articular surface has a clear subdued ridge that is not like that described in the proximal metatarsal base from Hadar, Ethiopia (A.L. 333-54) wherein a distinct elevation nearly bisects the articular base into two semicircular facets[14] and in doing so, acts to immobilize the joint by effectively negating any conjunct axial rotation of the hallux. The articular head, when viewed laterally, is distinctly flattened on its dorsal surface and extends only minimally above the diaphyseal surface. In dorsal view, the distal articular surface is asymmetrically beveled and flattened so that it is directed anteromedially. In lateral view, the shaft is curved directing the head plantarward. There is a slight torsion of the head toward the lateral side of the foot. It is notable that the BRT-VP-2/73c hallucal metatarsal head fails to conform to the "typical" *Australopithecus* pattern in that it lacks the dramatic dorsal doming that characterizes this genus[6,16].

The doming of the hallucal metatarsal head is among the most discriminating morphological characteristics that define the genus *Australopithecus*[6,14,16]. This feature is highly significant functionally in that it indicates the extended range of passive dorsiflexion necessary at

bipedal toe-off and the utilization of the "transverse" metatarsal axis (see Refs 11, 14 for additional discussion). It also signals the permanent adduction of the great toe, the formation of a permanent longitudinal arch and the complete forfeiture of ape-like hallucal abduction[11,14]. In lacking this important feature BRT-VP-2/73c is dissimilar to the contemporaneous *Au. afarensis* and instead exhibits a morphological pattern more like that seen in *Ardipithecus ramidus*[11].

The ratio formed by comparing the first and second metatarsal lengths to the fourth metatarsal length also shows that the hallucal element is unexpectedly short wherein it falls outside of the ranges of both the African apes and humans and instead resembles extant monkeys.

2.2. The second ray

The shaft of the second metatarsal is transversely fractured in three places but these appose cleanly and do not distort the original morphology. There is some minor abrasion damage on the base and head. The tubercles for the collateral ligaments are asymmetrical with the lateral being the larger and more proximately situated. The proximal base is triangular in outline with deep ligamentous excavations on its lateral margin.

2.3. The fourth ray

The fourth metatarsal is essentially complete with some surface abrasion on the proximal and distal articular surfaces. A well-apposed crack occurs through the distal third of the shaft but this does not adversely affect its natural morphology. Although areas of the subchondral surface of the metatarsal head are abraded the remaining trabecular bone preserves the rounded triangular outline of the head in distal view. In lateral view, this bone is surprisingly straight. The *Australopithecus* and *Ardipithecus*-like dorsal doming of the distal articular surface is obvious. On the dorsomedial side of the head, the subchondral surface continues proximally onto the

medial tubercle largely obliterating the characteristic transverse gutter. The medial tubercle is more distally located on the shaft than is the lateral. There is slight axial torsion along the shaft that results in the metatarsal head facing somewhat laterally relative to its base. This torsion occurs in hominids and cercopithecines but not in the African apes (see Supp. Figure 2; see also Ref. 12) and indicates a transverse pedal arch. This is likely a primitive feature as it is not seen in the African apes owing to their highly derived, abducent halluces and enhanced midfoot laxity.

However, when viewed from above it does exhibit a slight bowing along the shaft such that the head is directed somewhat laterally, a condition similar to that seen in Old World Monkeys and quite different from the medial torsion observed in the African apes[12]. The proximal joint surface for the lateral cuneiform is flat. Although damaged on its plantar margin, it does not appear to have the dorsoplantarly expanded base described in *Australopithecus afarensis*[12].

The proximal phalanx of the fourth ray is complete. Its proximal articular surface is canted anteriorly indicating, in combination with the accompanying domed metatarsal head, the ability to achieve the passive hyperdorsiflexion of the metatarsophalangeal joint necessary for bipedal toe-off. The shaft is strongly curved, another feature that characterizes early hominid proximal phalanges[11,14,16] (see ref. 11 for discussions).

The earlier *Ar. ramidus* pedal remains dramatically demonstrate a compromise foot capable of terrestrial bipedal toeing-off on the lateral four metatarsophalangeal joints (oblique metatarsal axis[11]) while still maintaining a functionally abductable, grasping hallux. This condition did not permit habitual toe-off on the great toe, nor did it allow the use of the "transverse metatarsal axis." Instead, it provided rigidity on the lateral side of its foot by maintaining a long midtarsus, dorsoplantarly expanded metatarsal bases, and an oblique

orientation of its *fibularis longus* tendon relative to the midtarsal axis[11]. It is clear that dorsal doming of the lateral four metatarsal heads and the canting of the proximal phalangeal bases are among the earliest pedal adaptations for hominid terrestrial bipedality. It is also apparent that a longitudinal pedal arch was not possible to maintain in the absence of the permanently adducted hallux indicating that this important energy dissipating mechanism[29] arose later.

Moreover, the base of the hallucal metatarsal suggests conjunct axial rotation and an abducent great toe. The South African hallucal metatarsals (StW 562, StW 595)[10] also fail to exhibit the distinctive doming of the metatarsal head and in this sense are similar to BRT-VP-2/73. Combined with the suggested hallucal abducence is the observation that the second metatarsal demonstrates axial torsion along its shaft so that the distal articular surface is facing medially toward the grasping hallux. This grasping complex more closely approximates the African apes and *Ar. ramidus* than it does later hominids. Similar medially directed torsion is also seen in the second metatarsal (StW 89) from Sterkfontein[10].

While failing to exhibit expanded metatarsal bases on the second and fourth rays, the BRT-VP-2/73 hallucal metatarsal base does exhibit an elongated dorsoplantar axis to its proximal base and in this feature it is similar to the African apes, humans, and other hominids and unlike Old World monkeys and Miocene apes (eg., KMN-RU 2036, ref. 17).

The asymmetrical flattening described for the hallucal metatarsal head suggests that the great toe was oriented in an abducted position during stance phase of the gait cycle. The toed-out foot placement would result in the abducted hallux being directed anteromedially, a position that led to the asymmetrical flattening of the head owing to the oblique directionality of the ground reaction vector. Importantly, the diminutive length of the great toe and the lack of dorsal doming

strongly suggest that the hallux did not play a significant propulsive role during toe-off but rather likely assisted in balancing. A similar functional scenario was described for *Ar. ramidus*[11].

Moreover, the shape of the lateral metatarsal heads, the asymmetry of the dorsal tubercles, and the angulation of the dorsal gutters also indicate that, like *A. ramidus* and *Au. afarensis*, loading during heel-off through toe-off occurred in a somewhat toed-out foot position. As a consequence of this foot placement during late toe-off, the metatarsals and hindfoot would rotate externally while the more distal elements (the phalanges) were stabilized by frictional forces against the substrate.

The lack of dorsoplantar expansion of the metatarsal bases (MT's 2, 4) in BRT-VP 2/73 suggests that this midtarsal stabilizing feature seen in both *Ar. ramidus*[11] and *Au. afarensis*[12] was absent in this specimen. Rather, enhanced midfoot laxity may have resulted in a "midtarsal break" during heel-off allowing closer plantar conformation to an arboreal substrate[19-22].

The relatively long fourth ray may have functionally altered the orientation of the oblique metatarsal axis suggesting that primary loading during the heel-off through toe-off phase of the gait cycle occurred principally through the third and forth rays rather than the second and third rays as it does in extant hominoids and as has been reconstructed for *Ar. ramidus*[11]. This combined with the significant torsion of the second metatarsal toward the hallux may indicate that the second metatarsal played a lesser role during toe-off than it did in either *A. ramidus* or in subsequent *Au. afarensis*. This may also be retention of the primitive, Miocene ape-like condition, but at present this remains irresolvable.

The inclusion of the BRT-VP-2/73 partial foot skeleton into the existing *Au. afarensis* morphological paradigm may expand this model beyond its useful limits. Clearly the functional adaptations seen in the BRT-VP-2/73 foot include a selectively significant amount of arboreal

behaviors. By contrast, the anatomical evidence for *Au. afarensis* is dramatic in its indication of an habitual biped that had forsaken selectively important levels of climbing.

3. Dorsal canting and curvature of proximal phalanges

Dorsal canting of the bases of the pedal proximal phalanges is the result of passive hyper-dorsiflection during the toe-off phase of the hominin gait cycle. This trait has been used as a diagnostic indicator of bipedality in early hominins (e.g., Ref. 14). As Griffin and Richmond[15] recently showed, canting of the base of pedal proximal phalanges is not uniquely hominin trait and that it is also seen in chimpanzees and gorillas with a variable degree of overlap, and even in some late Miocene hominoid taxa[30].

Several semi-digitigrade and digitigrade mammals do, indeed, have dorsally canted bases to their proximal phalanges, largely for the same functional reason, hyper-dorsiflexion at the latter stages of toe-off. However, to imply that these morphologies are somehow similar to a hominin-like functional complex is overly simplistic and seriously mistaken. The dorsally canted phalangeal bases must be viewed, not in isolation but within the overall context of the metatarsophalangeal articulation. The canting of the phalangeal bases in combination with the dorsal doming of the hominin metatarsal heads indicates an expanded range of passive dorsiflexion necessary during hominin bipedal toe-off. We agree that canted phalangeal bases occur in other mammals with diverse locomotor patterns. However, when seen within the functional context of a hominin plantigrade foot, it is clear that hominin metatarsophalangeal joints are both functionally and anatomically distinct..

The degree of dorsal canting is highly variable and some overlap is apparent across various primate taxa. However, hominins tend to show hyperdorsiflection necessary for bipedal heel-off through toe-off. More importantly, dorsal canting of the phalangeal bases cannot be

taken out of functional context. The morphology and functions of the hominin metatarsophalangeal articulations are unique and are easily identified. Simply measuring the dorsal cant of the phalangeal base and comparing this isolated metric among various species per se is not functionally informative.

Dorsal canting on the BRT-VP-2/73 second and fourth proximal phalanges were measured using the simple technique applied by Griffin and Richmond[15]. These measurements fall in the range of modern humans sampled by Griffin and Richmond[15], indicating that the BRT foot was derived toward bipedal hominins in these measures (Supp. Figure 4a). Curvature of the proximal phalanges of BRT-VP-2/73 indicates that this foot was perhaps better suited for arboreal repertoire than are gorillas and humans. The included angle measurement on the BRT foot proximal phalanges is 29º, falling within the range documented for *Au. afarensis* and lower range of chimpanzees[31] (see Supp. Figure 4b for comparative illustration). Chimpanzees on average have the most curved proximal phalanges due to their extreme arboreality.

4. Principal Component Analysis (PCA)

A Principal Component Analysis (PCA; correlation matrix, varimax rotation with Kaiser normalization) was conducted on eleven metatarsal ratios (see Supp. Table 1). The two extracted components explain 77.3% of the total variance where PC1 and PC2 account for 41.2% and 36.2%, respectively. The Eigenvalue for PC1 is 7.095 and 1.411 for PC2. Principal components 1 and 2 are presented in Supplementary Table 9. Almost all of the ratios significantly contribute to the variation. However, ratios 6, 9, and 10 appear to account for most of the variation. These ratios are exclusively related to the hallucal metatarsal. PC1 discriminates monkeys from African apes and humans; BRT-VP-2/73 falls in the African ape and human cloud. PC2 also clearly discriminates monkeys from the African apes and humans but, in combination with PC1, also

separates chimpanzees from gorillas and humans, with BRT-VP-2/73 falling in the gorilla/human cloud. It is interesting that humans and gorillas substantially overlap (to the exclusion of chimpanzees) in the ratios considered in this analysis calling for further investigation.

5. Fauna and paleoenvironment

The BRT faunal assemblage represents varied habitats along a lakeshore or river floodplain similar to penecontemporaneous eastern African sites such as Hadar[32] and Lomekwi[33]. However, it is difficult at this time to conclusively infer the paleoenvironment at BRT, or its similarities and differences to other contemporaneous site in eastern Africa, based on the fauna alone, largely due to the small sample size (see Supplementary Information and Supplementary Table 5, for details). However, the mammalian faunal assemblage from the two Burtele (BRT) localities is diverse relative to the number of specimens collected (n = 195, see Supplementary Table 5). It is largely dominated by bovids and among these, aepycerotines, gazelle-like antilopines, and alcelaphines are the most abundant. Tragelaphines, reduncines, hippotragines, neotragines, and bovines are rare. Suids are represented by three species: *Nyanzachoerus kanamensis*, *Notochoerus euilus*, and *Kolpochoerus* cf. *afarensis*. Among the primates, *Theropithecus oswaldi* spp. is present. One specimen has also been identified as Galagidae. *Diceros* sp. and *Elephas recki* spp. represent the large mammals. Carnivores are rare at both localities with only cf. Hyaenidae and a species of herpestid identified thus far. Tragelaphines prefer woodlands and bushlands while reduncines prefer swamps or grassy wetlands with abundant water[34]. The relative abundance of aepycerotines and alcelaphines at BRT indicates the presence of drier woodlands and grasslands[34]. The presence of gastropods and aquatic vertebrate taxa (e.g., fish, crocodiles, hippopotamus), within a progradational deltaic depositional environment, suggests the presence of a large body of perennial water in the area. Therefore,

preliminary habitat indications based on the available fauna suggest that the BRT localities represent both open country and wooded habitats, with indications of locally well-watered environments, which is consistent with the sedimentological indications of a deltaic system.

Isotopic analysis of paleosol samples from two horizons within the BRT section provide additional indication of the environmental context for the BRT sediments. Pedogenic carbonates were sampled from two vertic paleosol strata that underlie the fossil foot site and represent terrestrial intervals at the top of progradational deltaic cycles. Two micritic carbonate nodules were analyzed from both the lower (WM11-BRT-140) and upper (WM11-BRT-141) paleosols. $\delta^{13}C$ values of these nodules average -13.7 ± 0.3‰ and -8.4 ± 0.4‰ for the lower and upper paleosols, respectively (Supplementary Table 8). Clumped-isotope derived temperatures indicate that soil temperatures were 37±6˚C and 31±2˚C for the lower and upper paleosols, respectively.

The carbon isotope results suggest that the lower paleosol supported a forested environment whereas the upper paleosol supported a woodland/bushland/shrubland environment, following the interpretive scheme in Cerling *et al*.[35]. In both cases, these strata represent landscapes that were dominated by C_3 plants during soil formation. The $\delta^{13}C$ values from the lower paleosol is unique in that it is lower than any other $\delta^{13}C$ value determined from pedogenic carbonates from the earliest late Pliocene strata in the neighboring Hadar Formation and in the Omo Group Sediments (Supplementary Table 10). The paleosol isotopic data represent the environments of stable land surfaces associated with the progradational delta system that were lateral to the deposition of the fossiliferous sands.

Supplementary Table 1. List of metatarsal ratios used in the Principal Component Analysis (PCA). Taxa used in this analysis are listed in Supplementary Table 6.

Ratio no.	Description
1	Hallucal metatarsal length to second metatarsal length
2	Hallucal metatarsal length to fourth metatarsal length
3	Second metatarsal length to fourth metatarsal length
4	Second metatarsal base height to second metatarsal length
5	hallucal metatarsal base height to hallucal metatarsal length
6	Hallucal head height to its base height
7	Hallucal base height to second metatarsal base height
8	Second metatarsal head height to its base height
9	Hallucal head breadth to its height
10	Hallucal base breadth to its height
11	Hallucal head height to hallucal length

Supplementary Table 2. Measurements of metatarsals used in the comparative analysis. All measurements are in mm.

Specimen no	Element	Length	Prox ML	Prox DP	Distal ML	Distal DP	Mshaft ML	Mshaft DP
A.L. 333-115a	MT1	-	-	-	17.5	17.3	-	-
A.L. 333-115d	MT4	-	-	-	9.5	14	-	-
A.L. 333-54	MT1	-	17.4	23.5			-	-
A.L.333-21	MT1	-	-	-	16	16.4*	-	-
A.L. 333-160	MT4	59.9	13.1	17.1	8.5	13.4	6.1	9.1
StW 89	MT2	60.3	10.5	11.6		6.8		5.8
StW 377	MT2	56.7		15.4			6.3	7.9
StW 562	MT1	48.8	15	24.7	18.8	15.2	10.4	10.7
StW 595	MT1	44.6	11.8	18.1	15.1	12.3	7.5	8
StW 596	MT4						8.4	7.7
SKX 5017	MT1	44.3	13.4	21.8	17.6	13.4	10.2	13
KNM-RU 2036	MT1 (R)	35.4	-	12.2	-	-	4.8	5.4
KNM-RU 2036	MT1 (L)	34.8	-	11.2	-	-	5.6	6.1
KNM-RU 2036	MT2	47.7	-	-	-	-	4.8	4.9
KNM-RU 2036	MT4	52.8	-	-	-	-	5.1	4.9
	MT1							
Cercopithecinae	Mean	33.8	9.2	9.4	7.2	6.6	4.8	4.3
(n = 59)	Min	23.5	6.2	6.0	5.1	4.4	3.2	2.8
	Max	45.5	13.6	13.9	11.3	10.1	7.6	6.3
	SD	5.6	1.7	1.9	1.4	1.3	1.0	0.9
Colobinae	Mean	39.7	11.0	11.1	8.9	7.6	5.7	4.8
(n = 13)	Min	34.0	8.5	7.6	7.3	6.6	4.3	4.3
	Max	57.6	15.4	16.8	12.2	10.8	8.8	7.4
	SD	7.3	2.2	2.8	1.8	1.6	1.4	1.1
Gorilla gorilla	Mean	62.3	16.9	27.2	17.0	17.4	13.8	11.3
(n = 14)	Min	52.0	13.7	21.9	12.6	13.8	10.8	8.5
	Max	68.1	18.6	30.6	20.1	19.0	16.5	13.7
	SD	5.5	1.7	3.0	2.2	1.8	1.8	1.6
Pan troglodytes	Mean	56.5	14.1	21.3	13.3	14.5	10.8	9.7
(n = 21)	Min	47.5	12.5	19.0	16.0	13.9	9.2	8.7
	Max	61.4	17.0	23.0	11.8	16.8	13.2	11.0
	SD	4.1	1.2	1.2	1.1	0.9	1.2	0.7
Homo sapiens	Mean	61.5	17.3	27.9	20.0	19.6	13.2	13.2
(n = 20)	Min	54.8	14.7	24.4	16.8	17.3	10.6	10.8
	Max	72.1	20.4	33.2	24.0	23.1	15.9	16.4
	SD	4.5	1.8	2.5	1.8	1.8	1.5	1.5

Supplementary Table 2 (cont)

	MT2						
Cercopithecinae	Mean	49.5	6.5	9.6	6.0	6.8	4.4	4.2
(n = 59)	Min	36.0	4.3	5.8	4.4	4.7	2.7	2.7
	Max	69.4	10.2	14.9	9.0	10.5	6.5	6.9
	SD	8.0	1.3	1.9	1.1	1.2	0.9	0.9
Colobinae	Mean	57.4	8.0	11.0	6.7	8.2	5.0	5.2
(n = 13)	Min	49.5	6.5	8.0	5.6	6.4	4.5	3.5
	Max	68.3	10.9	15.2	9.0	10.7	6.8	6.6
	SD	6.3	1.5	2.3	1.1	1.4	0.8	1.0
Gorilla gorilla	Mean	81.9	17.1	19.2	12.2	15.2	9.9	12.5
(n = 14)	Min	72.0	13.1	15.0	9.4	12.7	7.8	8.5
	Max	88.9	19.2	22.2	12.9	16.8	12.0	14.0
	SD	5.7	1.7	2.1	1.1	1.1	1.2	1.7
Pan troglodytes	Mean	74.2	14.0	15.4	9.5	13.5	7.4	9.2
(n = 21)	Min	64.1	12.6	12.9	8.4	12.2	0.0	8.3
	Max	82.6	15.6	18.1	11.1	16.2	8.9	10.9
	SD	4.3	0.8	1.2	0.7	1.2	1.9	0.8
Homo sapiens	Mean	76.7	15.0	19.4	10.6	15.3	8.0	8.9
(n = 19)	Min	64.8	11.9	16.1	8.5	13.5	6.5	7.0
	Max	83.4	18.0	22.5	11.9	17.8	9.8	11.0
	SD	5.7	1.8	1.8	1.0	1.1	0.9	0.9
	MT4							
Cercopithecinae	Mean	51.9	6.4	9.3	6.8	7.6	4.2	4.4
(n = 59)	Min	37.8	4.1	6.4	5.0	5.1	2.9	3.0
	Max	72.3	10.4	15.4	10.2	11.6	6.8	6.3
	SD	8.4	1.3	2.1	1.2	1.3	0.9	0.8
Colobinae	Mean	63.1	7.4	10.7	7.6	8.9	4.9	5.3
(n = 13)	Min	50.8	4.9	8.6	6.5	7.5	4.1	4.0
	Max	72.6	10.9	14.7	10.3	11.4	6.1	6.9
	SD	6.7	1.6	2.0	1.1	1.4	0.8	0.9

Supplementary Table 2 (cont)

Gorilla gorilla	Mean	78.1	14.9	16.1	10.9	16.0	8.7	10.6
(n = 14)	Min	67.7	12.7	12.4	7.8	13.2	7.0	7.8
	Max	85.1	17.9	18.6	12.1	17.6	9.6	12.6
	SD	6.4	1.7	2.2	1.2	1.5	0.7	1.3
Pan troglodytes	Mean	67.6	11.5	12.9	8.4	14.9	6.4	7.4
(n = 21)	Min	55.5	9.2	11.1	7.1	13.0	5.4	6.7
	Max	76.0	13.2	16.4	9.9	16.3	8.1	8.7
	SD	4.5	1.2	1.1	0.7	1.0	0.7	0.5
Homo sapiens	Mean	69.8	11.9	16.4	9.6	14.2	9.5	8.5
(n = 20)	Min	59.8	10.4	14.0	7.9	12.5	7.7	6.8
	Max	77.0	14.0	19.6	10.0	17.1	11.2	10.4
	SD	5.4	1.0	1.5	0.6	1.0	0.8	1.1

Supplementary Table 3. Linear measurements (mm) and ratios of proximal and intermediate phalanges.

Specimen		M1	M2	M3	M4	R1	R2	R3
BRT-VP-2/73		25.2	29.7	28.7	18.5	0.50	0.44	0.78
Cercopithecinae (n=11)	Mean	16.0	23.5	27.4	-	0.43	0.48	0.75
	Min	12.9	18,9	-	-	0.37	0.46	0.65
	Max	20.6	26.2	-	-	0.50	0.55	0.76
	SD	2.4	3.2	-	-	0.04	0.03	0.04
Pan troglodytes (n=17)	Mean	28.8	36.6	40.2	23.1	0.52	0.49	0.77
	Min	25.1	31.1	35.2	18.5	0.45	0.45	0.71
	Max	31.9	41.5	43.1	24.9	0.56	0.55	0.82
	SD	2.0	2.4	1.9	2.4	0.03	0.03	0.03
Gorilla gorilla (n=9)	Mean	29.3	38.9	43.2	22.7	0.46	0.47	0.75
	Min	20.6	31.7	35	18.6	0.39	0.42	0.66
	Max	32.2	42.7	45.1	26.7	0.50	0.50	0.80
	SD	4.3	3.5	4.0	2.6	0.04	0.02	0.04
Homo sapiens (n=15)	Mean	31.1	26.5	23.2	13.9	0.49	0.35	0.91
	Min	27.3	22.6	20	11.2	0.43	0.34	0.84
	Max	33.6	31.1	26.2	18.2	0.52	0.40	0.98
	SD	1.8	2.1	1.8	1.9	0.02	0.01	0.04

M1, Ray 1 proximal phalanx length. **M2**, Ray 2 proximal phalanx length. **M3**, Ray 4 proximal phalanx length. **M4**, Ray 2 intermediate phalanx length. **R1**, Ratio of ray 1 proximal phalanx length to the length of the first metatarsal. **R2**, Ratio of ray 2 proximal phalanx length to the length of the second metatarsal. **R3,** Combined length of the first metatarsal and its proximal phalanx relative to the length of the second metatarsal and associated proximal phalanx.

Supplementary Table 4. Summary $^{40}Ar/^{39}Ar$ results.

Sample	Lab ID#	Mineral		Ca/K ± 1s SD	Age (Myr ago) ± 1s MSE		MSWD	Prob.	n/ntotal
WM07/B-1	25032, 25033	K-feldspar	0.035	0.002	3.484	0.011	1.3	0.15	24/30
WM10/B-1	25484	K-feldspar	0.034	0.002	3.453	0.011	1.0	0.40	4/4
WM10/B-1	25484	Plagioclase	2.5	0.3	3.42	0.03	1.1	0.33	18/22
				Overall weighted mean =	**3.469**	**0.008**			

Supplementary Table 5. Preliminary faunal list of BRT-VP-1 and BRT-VP-2.

Aves
- Gen et sp. indet.

Mammalia
- Primates
  - Hominidae
    - *Australopithecus cf. afarensis*
    - *Australopithecus sp. indet.*
  - Cercopithecidae
    - Colobinae
      - Gen et sp. indet.
    - Cercopithecinae
      - *Theropithecus oswaldi* spp.
  - Galagidae
    - cf. *Galago* sp. indet.
- Carnivora
  - Felidae
    - Machairodontinae
      - cf. *Homotherium* sp.
  - Hyaenidae
    - Gen. et sp. indet.
  - Herpestidae
    - Gen. et sp. indet.
- Artiodactyla
  - Bovidae
    - Aepycerotini
      - *Aepyceros* sp. indet
    - Alcelaphini
      - *Damaliscus* sp.
    - Tragelaphini
      - *Tragelaphus* spp.
    - Bovini
    - Hippotragini
      - *Hippotragus* sp.
    - Antilopini
      - *Gazella* sp.
    - Neotragini
    - Reduncini
  - Suidae
    - *Notochoerus euilus*
    - *Nyanzachoerus kanamensis*
    - *Kolpochoerus cf. afarensis*
- Perissodactlya
  - Equidae
    - *Eurgnathohippus* sp.
  - Rhinocerotidae
    - *Diceros* sp.
- Proboscidea
  - Elephantidae
    - *Elephas recki* subsp. Indet.
- Rodentia
  - Thryonomyidae
    - *Thryonomys* sp.

Supplementary Table 6. Taxonomic composition of modern primate taxa used in the comparative analysis presented in Figure 3 of the main text. Numbers in parentheses indicate the number of individual elements measured from each taxon.

Cercopithecinae	Colobinae	Panini
Cercocebus agilis (5)	*Colobus guereza* (2)	*Pan troglodytes* (21)
Cercocebus Torquatus (6)	*Erythrocebus patas* (3)	
Cercopithecus mitis (5)	*Mandrillus sphinx* (3)	
Cercopithecus neglectus (2)	*Mandrillus laecophaeus* (3)	**Gorillini**
Chlorocebus aethiops (7)	*Nasalis lavratus* (4)	*Gorilla gorilla* (15)
Lophocebus albigena (4)	*Presbytis melalophos* (1)	
Macaca fasicularis (4)	*Semnopithecus entellus* (2)	
Macaca nemestrina (7)		**Hominini**
Macaca thibetana (4)		*Homo sapiens* (19)
Papio anubis (5)		
Theropithecus gelada (5)		

doi:10.1038/nature10922

Supplementary Table 7. $^{40}Ar/^{39}Ar$ analytical data.

Lab ID#	Sample	Irrad.	*J* (X 10^{-3}) ± 1s		Relative Isotopic Abundances									
					^{40}Ar	±1s	^{39}Ar	±1s	^{38}Ar	±1s	^{37}Ar	±1s	^{36}Ar	±1s
WM10/B-1														
25484-02	WM10/B-1	392a	1.304	0.003	129.04	0.17	79.81	0.12	0.958	0.014	0.408	0.014	0.0378	0.0016
25484-12	WM10/B-1	392a	1.304	0.003	172.5	0.2	95.26	0.12	1.161	0.017	0.441	0.016	0.109	0.002
25484-22	WM10/B-1	392a	1.304	0.003	217.8	0.3	106.84	0.13	1.339	0.014	0.538	0.016	0.208	0.002
25484-24	WM10/B-1	392a	1.304	0.003	172.2	0.2	101.77	0.14	1.229	0.017	0.448	0.015	0.0787	0.0019
WM10/B-1 2														
25484-01	WM10/B-1	392a	1.304	0.003	20.38	0.07	12.07	0.03	0.134	0.004	3.76	0.05	0.0137	0.0014
25484-04	WM10/B-1	392a	1.304	0.003	27.70	0.07	15.03	0.03	0.183	0.005	3.85	0.07	0.0248	0.0015
25484-06	WM10/B-1	392a	1.304	0.003	18.52	0.05	10.62	0.03	0.126	0.003	3.50	0.03	0.0115	0.0014
25484-07	WM10/B-1	392a	1.304	0.003	13.63	0.04	7.94	0.02	0.096	0.004	2.99	0.04	0.0072	0.0016
25484-08	WM10/B-1	392a	1.304	0.003	16.92	0.05	10.22	0.03	0.122	0.004	3.49	0.04	0.0107	0.0015
25484-10	WM10/B-1	392a	1.304	0.003	26.70	0.08	16.08	0.04	0.193	0.005	5.37	0.05	0.0138	0.0015
25484-11	WM10/B-1	392a	1.304	0.003	18.22	0.05	10.61	0.02	0.138	0.004	3.31	0.03	0.0125	0.0015
25484-13	WM10/B-1	392a	1.304	0.003	19.64	0.07	11.09	0.03	0.134	0.007	3.70	0.04	0.0174	0.0015
25484-14	WM10/B-1	392a	1.304	0.003	12.35	0.03	7.27	0.03	0.092	0.005	2.72	0.02	0.0102	0.0015
25484-16	WM10/B-1	392a	1.304	0.003	26.16	0.08	11.93	0.03	0.172	0.005	4.25	0.02	0.0339	0.0017
25484-18	WM10/B-1	392a	1.304	0.003	18.53	0.06	10.06	0.03	0.128	0.005	3.18	0.07	0.0174	0.0015
25484-19	WM10/B-1	392a	1.304	0.003	15.22	0.05	9.18	0.03	0.115	0.005	3.13	0.03	0.0078	0.0015
25484-20	WM10/B-1	392a	1.304	0.003	8.28	0.03	4.700	0.019	0.060	0.004	1.708	0.020	0.0050	0.0015
25484-21	WM10/B-1	392a	1.304	0.003	18.28	0.07	10.95	0.03	0.138	0.004	5.11	0.08	0.0140	0.0016
25484-23	WM10/B-1	392a	1.304	0.003	12.91	0.05	7.361	0.019	0.097	0.005	3.21	0.04	0.0106	0.0015
25484-25	WM10/B-1	392a	1.304	0.003	11.07	0.04	6.296	0.018	0.078	0.004	2.17	0.02	0.0093	0.0014
25484-26	WM10/B-1	392a	1.304	0.003	19.60	0.06	10.95	0.02	0.132	0.004	3.42	0.04	0.0178	0.0014
25484-27	WM10/B-1	392a	1.304	0.003	17.64	0.06	9.75	0.03	0.112	0.006	3.48	0.04	0.0130	0.0014
Omitted, 1.5 nMADs from median age:														
25484-05	WM10/B-1	392a	1.304	0.003	11.86	0.05	6.58	0.02	0.085	0.005	2.92	0.03	0.0072	0.0015
25484-09	WM10/B-1	392a	1.304	0.003	13.99	0.04	7.74	0.02	0.098	0.004	3.51	0.04	0.0079	0.0015
25484-17	WM10/B-1	392a	1.304	0.003	9.52	0.05	4.79	0.02	0.066	0.003	1.851	0.018	0.0066	0.0016

Supplementary Table 7 (cont)

Omitted, <60 %40Ar*:													
25484-15	WM10/B-1	392a	1.304	0.003	32.77	0.07	12.85	0.03	0.181	0.005	3.94	0.05	0.0503	0.0017
WM07/B-1														
25032-01	WM07/B-1	372A	1.344	0.003	14.91	0.02	10.243	0.012	0.121	0.002	0.083	0.009	0.0014	0.0007
25032-02	WM07/B-1	372A	1.344	0.003	28.12	0.04	19.197	0.019	0.232	0.003	0.156	0.009	0.0025	0.0007
25032-04	WM07/B-1	372A	1.344	0.003	15.12	0.04	10.620	0.019	0.133	0.002	0.086	0.009	0.0000	0.0007
25032-05	WM07/B-1	372A	1.344	0.003	21.73	0.05	14.80	0.03	0.180	0.004	0.110	0.009	0.0018	0.0008
25032-07	WM07/B-1	372A	1.344	0.003	15.83	0.03	10.95	0.03	0.142	0.004	0.082	0.009	0.0000	0.0008
25032-08	WM07/B-1	372A	1.344	0.003	21.63	0.05	11.603	0.017	0.145	0.003	0.099	0.009	0.0154	0.0008
25032-09	WM07/B-1	372A	1.344	0.003	25.89	0.04	17.50	0.02	0.213	0.003	0.129	0.009	0.0020	0.0008
25032-11	WM07/B-1	372A	1.344	0.003	27.22	0.05	18.31	0.03	0.215	0.004	0.174	0.009	0.0029	0.0008
25032-13	WM07/B-1	372A	1.344	0.003	29.24	0.05	19.90	0.03	0.246	0.004	0.154	0.009	0.0014	0.0009
25032-14	WM07/B-1	372A	1.344	0.003	18.22	0.03	10.66	0.03	0.130	0.002	0.079	0.009	0.0091	0.0009
25032-15	WM07/B-1	372A	1.344	0.003	29.08	0.06	19.52	0.03	0.239	0.004	0.149	0.009	0.0026	0.0009
25032-16	WM07/B-1	372A	1.344	0.003	19.42	0.04	13.25	0.02	0.167	0.002	0.095	0.009	0.0000	0.0009
25032-17	WM07/B-1	372A	1.344	0.003	26.43	0.05	18.39	0.03	0.216	0.003	0.154	0.009	0.0002	0.0009
25032-18	WM07/B-1	372A	1.344	0.003	21.49	0.06	14.44	0.04	0.176	0.004	0.115	0.009	0.0015	0.0009
25032-19	WM07/B-1	372A	1.344	0.003	15.63	0.03	10.87	0.04	0.124	0.003	0.089	0.009	0.0000	0.0009
25032-20	WM07/B-1	372A	1.344	0.003	26.16	0.04	17.65	0.03	0.224	0.004	0.125	0.009	0.0005	0.0009
25032-21	WM07/B-1	372A	1.344	0.003	21.35	0.04	14.58	0.03	0.180	0.003	0.108	0.009	0.0006	0.0009
25032-24	WM07/B-1	372A	1.344	0.003	22.90	0.05	15.51	0.03	0.189	0.005	0.113	0.009	0.0012	0.0009
25033-01	WM07/B-1	372A	1.345	0.003	59.32	0.08	40.01	0.07	0.467	0.005	0.324	0.009	0.0069	0.0009
25033-02	WM07/B-1	372A	1.345	0.003	43.21	0.08	27.91	0.06	0.334	0.007	0.214	0.009	0.0121	0.0009
25033-03	WM07/B-1	372A	1.345	0.003	31.03	0.05	21.62	0.05	0.267	0.005	0.171	0.009	0.0002	0.0008
25033-04	WM07/B-1	372A	1.345	0.003	17.71	0.04	11.85	0.02	0.144	0.004	0.086	0.009	0.0017	0.0008
25033-05	WM07/B-1	372A	1.345	0.003	55.17	0.06	27.50	0.05	0.341	0.005	0.210	0.009	0.0553	0.0009
25033-06	WM07/B-1	372A	1.345	0.003	36.84	0.06	24.37	0.04	0.299	0.005	0.204	0.009	0.0079	0.0008
Omitted, 1.5 nMADs from median age:														
25032-03	WM07/B-1	372A	1.344	0.003	16.19	0.04	11.35	0.02	0.140	0.002	0.091	0.009	0.0009	0.0007
25032-12	WM07/B-1	372A	1.344	0.003	14.40	0.03	7.39	0.03	0.094	0.003	0.055	0.009	0.0101	0.0009
25032-22	WM07/B-1	372A	1.344	0.003	14.28	0.03	9.44	0.02	0.111	0.003	0.072	0.009	0.0006	0.0009

Supplementary Table 7 (cont)

Omitted, <60 %40Ar*:														
25032-06	WM07/B-1	372A	1.344	0.003	22.46	0.05	8.280	0.017	0.113	0.003	0.065	0.009	0.0347	0.0008
25032-10	WM07/B-1	372A	1.344	0.003	103.74	0.09	15.18	0.02	0.231	0.004	0.137	0.009	0.2749	0.0013
25032-23	WM07/B-1	372A	1.344	0.003	43.88	0.06	15.82	0.02	0.212	0.004	0.146	0.009	0.0687	0.0010

Supplementary Table 7 (cont, second panel)

Lab ID#	Sample	Irrad.	Derived Results									
			^{39}Ar Mol ¥ 10^{-14}	%(36Ar)Ca	Ca/K ±1s		$^{40}Ar^{*}/^{39}Ar$ ±1s		%$^{40}Ar^{*}$	Age (Ma) ±1s		w/±*J* ±1s
WM10/B-1												
25484-02	WM10/B-1	392a	2.79	1.0	0.0363	0.0012	1.4775	± 0.0073	91.4	3.473	0.017	0.02
25484-12	WM10/B-1	392a	3.33	0.4	0.0331	0.0012	1.4724	± 0.0082	81.4	3.461	0.019	0.02
25484-22	WM10/B-1	392a	3.73	0.2	0.0362	0.0011	1.4622	± 0.0079	71.8	3.437	0.018	0.02
25484-24	WM10/B-1	392a	3.55	0.5	0.0317	0.0011	1.4635	± 0.0073	86.6	3.440	0.017	0.02
					0.034	**0.002**	**1.4689**	**± 0.0038**		**3.453**	**0.009**	**0.011**
WM10/B-1 2												
25484-01	WM10/B-1	392a	0.42	26.3	2.20	0.03	1.4416	± 0.0350	85.4	3.39	0.08	0.08
25484-04	WM10/B-1	392a	0.52	14.9	1.82	0.04	1.4269	± 0.0308	77.4	3.35	0.07	0.07
25484-06	WM10/B-1	392a	0.37	29.2	2.34	0.02	1.5170	± 0.0412	87.0	3.56	0.10	0.10
25484-07	WM10/B-1	392a	0.28	40.1	2.68	0.04	1.5574	± 0.0594	90.7	3.66	0.14	0.14
25484-08	WM10/B-1	392a	0.36	31.3	2.43	0.03	1.4431	± 0.0449	87.1	3.39	0.10	0.11
25484-10	WM10/B-1	392a	0.56	37.4	2.38	0.02	1.5012	± 0.0281	90.4	3.53	0.07	0.07
25484-11	WM10/B-1	392a	0.37	25.6	2.226	0.018	1.4576	± 0.0419	84.9	3.42	0.10	0.10
25484-13	WM10/B-1	392a	0.39	20.5	2.38	0.03	1.4010	± 0.0412	79.1	3.29	0.10	0.10
25484-14	WM10/B-1	392a	0.25	25.7	2.67	0.02	1.3894	± 0.0624	81.8	3.26	0.15	0.15
25484-16	WM10/B-1	392a	0.42	12.2	2.555	0.017	1.4569	± 0.0432	66.4	3.42	0.10	0.10
25484-18	WM10/B-1	392a	0.35	17.7	2.26	0.05	1.4216	± 0.0452	77.2	3.34	0.11	0.11
25484-19	WM10/B-1	392a	0.32	39.2	2.45	0.02	1.5061	± 0.0484	90.8	3.54	0.11	0.11
25484-20	WM10/B-1	392a	0.16	33.4	2.61	0.03	1.5546	± 0.0975	88.2	3.6	0.2	0.23
25484-21	WM10/B-1	392a	0.38	35.5	3.36	0.05	1.4276	± 0.0435	85.4	3.36	0.10	0.10
25484-23	WM10/B-1	392a	0.26	29.4	3.14	0.04	1.4539	± 0.0608	82.8	3.42	0.14	0.14
25484-25	WM10/B-1	392a	0.22	22.7	2.49	0.02	1.4200	± 0.0681	80.7	3.34	0.16	0.16
25484-26	WM10/B-1	392a	0.38	18.8	2.25	0.02	1.4011	± 0.0397	78.3	3.29	0.09	0.09
25484-27	WM10/B-1	392a	0.34	26.2	2.58	0.03	1.5197	± 0.0442	84.0	3.57	0.10	0.10
					2.5	**0.3**	**1.4609**	**± 0.0102**		**3.42**	**0.03**	**0.03**
Omitted, 1.5 nMADs from median age:												
25484-05	WM10/B-1	392a	0.23	38.9	3.15	0.04	1.6042	± 0.0685	89.0	3.77	0.16	0.16
25484-09	WM10/B-1	392a	0.27	43.0	3.23	0.03	1.6357	± 0.0577	90.5	3.84	0.14	0.14
25484-17	WM10/B-1	392a	0.17	27.2	2.77	0.03	1.6902	± 0.0980	85.1	4.0	0.2	0.23

Supplementary Table 7 (cont, second panel)

Omitted, <60 %40Ar*:												
25484-15	WM10/B-1	392a	0.45	7.6	2.19	0.03	1.4812	± 0.0404	58.1	3.48	0.09	0.10
WM07/B-1												
25032-01	WM07/B-1	372A	0.63	3.5	0.036	0.004	1.4154	± 0.0216	97.3	3.43	0.05	0.05
25032-02	WM07/B-1	372A	1.18	3.6	0.036	0.002	1.4267	± 0.0119	97.4	3.45	0.03	0.03
25032-04	WM07/B-1	372A	0.65	0.0	0.036	0.004	1.4267	± 0.0212	100.2	3.45	0.05	0.05
25032-05	WM07/B-1	372A	0.91	3.6	0.033	0.003	1.4332	± 0.0159	97.6	3.47	0.04	0.04
25032-07	WM07/B-1	372A	0.67	0.0	0.033	0.004	1.4677	± 0.0223	101.6	3.55	0.05	0.05
25032-08	WM07/B-1	372A	0.71	0.4	0.038	0.003	1.4738	± 0.0222	79.1	3.57	0.05	0.05
25032-09	WM07/B-1	372A	1.08	3.7	0.033	0.002	1.4460	± 0.0142	97.7	3.50	0.03	0.04
25032-11	WM07/B-1	372A	1.13	3.6	0.042	0.002	1.4411	± 0.0142	97.0	3.49	0.03	0.03
25032-13	WM07/B-1	372A	1.22	6.7	0.034	0.002	1.4493	± 0.0138	98.7	3.51	0.03	0.03
25032-14	WM07/B-1	372A	0.66	0.5	0.033	0.004	1.4565	± 0.0261	85.3	3.53	0.06	0.06
25032-15	WM07/B-1	372A	1.20	3.4	0.034	0.002	1.4502	± 0.0145	97.4	3.51	0.04	0.04
25032-16	WM07/B-1	372A	0.81	0.0	0.032	0.003	1.4677	± 0.0208	100.2	3.55	0.05	0.05
25032-17	WM07/B-1	372A	1.13	52.5	0.037	0.002	1.4354	± 0.0154	99.9	3.48	0.04	0.04
25032-18	WM07/B-1	372A	0.89	4.6	0.036	0.003	1.4580	± 0.0201	98.0	3.53	0.05	0.05
25032-19	WM07/B-1	372A	0.67	0.0	0.037	0.004	1.4526	± 0.0255	101.1	3.52	0.06	0.06
25032-20	WM07/B-1	372A	1.08	14.5	0.032	0.002	1.4745	± 0.0157	99.5	3.57	0.04	0.04
25032-21	WM07/B-1	372A	0.90	10.9	0.033	0.003	1.4534	± 0.0186	99.3	3.52	0.04	0.05
25032-24	WM07/B-1	372A	0.95	5.4	0.033	0.003	1.4532	± 0.0173	98.5	3.52	0.04	0.04
25033-01	WM07/B-1	372A	2.46	2.8	0.0365	0.0011	1.4326	± 0.0079	96.7	3.472	0.019	0.02
25033-02	WM07/B-1	372A	1.72	1.1	0.0345	0.0015	1.4203	± 0.0108	91.8	3.44	0.03	0.03
25033-03	WM07/B-1	372A	1.33	47.0	0.0356	0.0019	1.4333	± 0.0123	99.9	3.47	0.03	0.03
25033-04	WM07/B-1	372A	0.73	3.0	0.033	0.003	1.4526	± 0.0211	97.3	3.52	0.05	0.05
25033-05	WM07/B-1	372A	1.69	0.2	0.0345	0.0015	1.4121	± 0.0132	70.4	3.42	0.03	0.03
25033-06	WM07/B-1	372A	1.50	1.6	0.0378	0.0017	1.4167	± 0.0111	93.7	3.43	0.03	0.03
					0.035	**0.002**	**1.4437**	**± 0.0030**		**3.484**	**0.008**	**0.011**
Omitted, 1.5 nMADs from median age:												
25032-03	WM07/B-1	372A	0.70	6.2	0.036	0.003	1.4048	± 0.0199	98.5	3.40	0.05	0.05
25032-12	WM07/B-1	372A	0.45	0.3	0.033	0.005	1.5455	± 0.0368	79.3	3.74	0.09	0.09
25032-22	WM07/B-1	372A	0.58	7.3	0.034	0.004	1.4948	± 0.0283	98.9	3.62	0.07	0.07

Supplementary Table 7 (cont, second panel)

Omitted, <60 %40Ar*:												
25032-06	WM07/B-1	372A	0.51	0.1	0.035	0.005	1.4756	± 0.0318	54.4	3.57	0.08	0.08
25032-10	WM07/B-1	372A	0.93	0.0	0.040	0.003	1.4832	± 0.0449	21.7	3.59	0.11	0.11
25032-23	WM07/B-1	372A	0.97	0.1	0.041	0.002	1.4920	± 0.0223	53.8	3.61	0.05	0.05

NOTES:
Samples were irradiated for five hours in two separate batches in the Cd-lined CLICIT position of the University of Oregon TRIGA reactor. Sanidine from the Fish Canyon Tuff was used as the neutron fluence monitor with a reference age of 28.201 Ma (Kuiper et al., 2008).

Nucleogenic production ratios:

(36Ar/37Ar)Ca	2.65	± 0.022	× 10-4
(39Ar/37Ar)Ca	6.95	± 0.092	× 10-4
(38Ar/37Ar)Ca	0.196	± 0.0082	× 10-4
(40Ar/39Ar)K	2.5	± 0.92	× 10-4
(38Ar/39Ar)K	1.22	± 0.0027	× 10-2
(36Ar/38Ar)Cl	3.2		× 102
37Ar/39Ar to Ca/K	1.96		

Isotopic constants and decay rates:

λ(40Kε) /yr		5.81	± 0.17 × 10-11
λ(40Kβ−) /yr		4.962	± 0.086 × 10-10
λ(37Ar) /d		1.975	× 10-2
λ(39Ar) /d		7.068	× 10-6
λ(36Cl) /d		6.308	× 10-9
(40Ar/36Ar)Atm	295.5		
(40Ar/38Ar)Atm	1575	± 2	
	40K/KTotal		0.01167

Supplementary Table 8. Stable isotope results from pedogenic carbonates.

Sample ID	N†	$\delta^{13}C$‡ ‰, PDB	$\delta^{18}O$‡ ‰, PDB	Δ_{47}§ ‰	Temperature†† (˚C)	$\delta^{18}O_{sw}$ ‰, SMOW
WM11-BRT-141A	2	-8.1 (0.01)	-3.1 (0.06)	0.619 (0.009)	31.3 (2.3)	0.5 (0.4)
WM11-BRT-141C	1	-8.7	-3.0	-	-	-
WM11-BRT-140A	1	-13.9	-0.7	0.592 (0.026)	37.9 (6.6)	4.2 (1.2)
WM11-BRT-140C	2	-13.5 (0.01)	-1.4 (0.02)	0.594 (0.023)	37.4 (5.8)	3.4 (1.1)

†Number of unique extractions and analyses of CO_2 from carbonate.

‡Reproducibility is <0.07‰ (1σ), based on long-term repeated measurements of in-house carbonate standards. 1σ external precision is listed in parentheses where N = 2.

§ Values relative to the Δ_{47} scale of Ghosh et al.[36], as described in Huntington et al.[37], and are normalized to a canonical heated gas intercept of -0.8453‰ relative to Oztech reference CO2. An acid correction factor of +0.081‰ was used to normalize these data to 25 C phosphoric acid reactions[30]. Error estimates are listed in parentheses. For N = 2, the error is estimated as the absolute difference between analyses (D = Δ47(1) -Δ47(2)) divided by the square root of 2. If D is less than 0.013‰, the long-term average D value for homogeneous carbonate standards analyzed using the same methods, a value of 0.013‰ is used for D. For N = 1, error is estimated as 0.026‰, the long-term 2σ precision for in-house carbonate standards analyzed multiple times.

††Calculated using the empirical Δ_{47} − Temperature relationship of Ghosh et al.[36]. Error estimates listed in parentheses.

‡‡Calculated soil water $\delta^{18}O$ using the $\delta^{18}O_{mineral} - \delta^{18}O_{water}$ − T relationship for calcite reported in Kim and O'Neil[38], where T is based on clumped isotope thermometry. Propagated error listed in parentheses.

Supplementary Table 9. Varimax rotated component matrix of the ratios used in the principal component analysis.

	PC1	PC 2
Ratio 1	0.386	0.617
Ratio 2	0.646	0.641
Ratio 3	0.762	0.479
Ratio 4	0.28	0.692
Ratio 5	0.524	0.779
Ratio 6	0.228	-0.749
Ratio 7	0.596	0.677
Ratio 8	0.85	0.41
Ratio 9	-0.895	0.069
Ratio 10	-0.522	-0.756
Ratio 11	0.908	0.325

Supplementary Table 10. Lowest $\delta^{13}C$ values reported from early late-Pliocene paleosol carbonate records in eastern Africa.

Site	Sample ID	Member	Formation	$\delta^{13}C$ (PDB)	Reference
Gona	GONJQ-022	Denen Dora	Hadar	-12.5	Ref. 35
Dikika	E03-2012	Sidi Hakoma	Hadar	-11.5	Ref. 35
Hadar	P1-58	Sidi Hakoma	Hadar	-7.3	Ref. 39
Nachukui	KN07WT-411	Kataboi	Nachukui	-9.1	Ref. 40
Koobi Fora	659	Lokochot	Koobi Fora	-10.6	Ref. 41
Shungura	ET04-OMO-318	B	Shungura	-10.1	Ref. 40

Supplementary References

29. Latimer, B. The Perils of Being Bipedal. *Ann. Biomed. Eng*. **33**, 3-6 (2005).

30. Wood, B. & Harrison, T. The evolutionary context of the first hominins. *Nature*, **470**, 347-352, doi:10.1038/nature09709 (2011).

31. Stern, J. T., Jungers, W. L. & Susman, R. L. Quantifying Phalangeal Curvature: An Empirical Comparison of Alternative Methods. *Am. J. Phys. Anthropol*. **97**, 1-10 (1995).

32. Reed, K. Paleoecological patterns at the Hadar hominin site, Afar Regional State, Ethiopia. *J. Hum. Evol.* **54**, 743-768 (2008).

33. Leakey *et al*. New hominin genus from eastern Africa shows diverse middle Pliocene lineages. *Nature* **410**, 433-440 (2001).

34. Kingdon, J. *East African Mammals: Bovids, vol. IIIC*. (University of Chicago Press, Chicago, 1982).

35. Cerling T. E. *et al*. Woody cover and hominin environments in the past 6 million years. *Nature* **476**, 51-56 (2011).

36. Ghosh, P. *et al*. ^{13}C–^{18}O bonds in carbonate minerals: A new kind of paleothermometer. *Geochim. Cosmochim. Acta*, **70**, 1439-1456 (2006).

37. Huntington, K. W. *et al*. Methods and limitations of 'clumped' CO^2 isotope (D47) analysis by gas-source isotope ratio mass spectrometry. *Journal of Mass Spectrometry*, **44**, 1318-1329 (2009).

38. Kim, S.-T. & O'Neil, J. R. Equilibrium and nonequilibrium oxygen isotope effects in synthetic carbonates, *Geochim. Cosmochim. Acta*, **61**, 3461-3475 (1997).

39. Aronson, J. L., Hailemichael, M. & Savin, S. M. Hominid environments at Hadar from paleosol studies in a framework of Ethiopian climate change, *J. Hum. Evol*. **55**, 532-550, doi:10.1016/j.jhevol.2008.04.004 (2008).

40. Levin, N. E., Brown, F. H., Behrensmeyer, A. K., Bobe, R. & Cerling, T. E. Paleosol carbonates from the Omo Group: isotopic records of local and regional environmental change in East Africa. *Paleogeogr. Paleoclimatol. Paleoecol.* **307**, 75-89, doi:10.1016/j.palaeo.2011.04.026 (2011).

41. Cerling, T. E., Bowman, J. R. & O'Neil, J. R. An isotopic study of a fluvial-lacustrine sequence: the Plio-Pleistocene Koobi Fora sequence, East Africa, *Palaeogeogr. Palaeoclimatol. Palaeoecol*. **63**, 335-356 (1988).